



Design, synthesis, biological evaluation and pharmacophore model analysis of novel tetrahydropyrrolo[3,4-c]pyrazol derivatives as potential TRKs inhibitors



Tianxiao Wu, Chu Zhang, Ruicheng Lv, Qiaohua Qin, Nian Liu, Wenbo Yin, Ruifeng Wang, Yin Sun, Xiaoyan Wang, Yixiang Sun, Dongmei Zhao*, Maosheng Cheng

Key Laboratory of Structure-Based Drug Design and Discovery, Ministry of Education, School of Pharmaceutical Engineering, Shenyang Pharmaceutical University, 103 Wenhua Road, Shenhe District, Shenyang, 110016, PR China

ARTICLE INFO

Article history:

Received 28 April 2021

Received in revised form

2 June 2021

Accepted 3 June 2021

Available online 15 June 2021

Keywords:

TRK inhibitors

Anticancer

Selectivity

Pharmacophore model

ABSTRACT

The tropomyosin receptor kinases TRKs are responsible for different tumor types which caused by *NTRK* gene fusion, and have been identified as a successful target for anticancer therapeutics. Herein, we report a potent and selectivity TRKs inhibitor **19m** through rational drug design strategy from a micromolar potency hit **17a**. Compound **19m** significantly inhibits the proliferation of TRK-dependent cell lines (Km-12), while it has no inhibitory effect on TRK-independent cell lines (A549 and THLE-2). Furthermore, kinases selectivity profiling showed that in addition to TRKs, compound **19m** only displayed relatively strong inhibitory activity on ALK. These data may indicate that compound **19m** has a good drug safety. Partial ADME properties were evaluated *in vitro* and *in vivo*. Compound **19m** exhibited a good AUC values and volume of distribution and low clearance in the pharmacokinetics experiment of rats. Finally, a pharmacophore model guided by experimental results is proposed. We hope this theoretical model can help researchers find type I TRK inhibitors more efficiently.

© 2021 Elsevier Masson SAS. All rights reserved.

1. Introduction

The tropomyosin receptor kinases (TRKs), a family of three receptor tyrosine kinases (RTKs), regulates cell differentiation, proliferation, survival and pain [1–5]. The three subtypes of the TRKs are TRKA, TRKB, and TRKC, which are encoded by *NTRK1*, *NTRK2*, and *NTRK3* gene [6]. As a transmembrane receptor proteins, TRKs contain an extracellular domain for binding ligand, a transmembrane domain and a small intercellular domain which comprised of approximately 70 amino acids before and 15 amino acids after the kinase domain [7,8]. The kinase domain of the TRKs is structurally conserved. TRKA, TRKB, and TRKC share more than 95% sequence identity in the active site where the protein interact directly with ATP [9]. The growth factors of neurotrophin family such as nerve growth factor (NGF), brain-derived neurotrophic factor (BDNF) and various neurotrophins (NTs) can activate TRKs, and different isoform is activated by different ligands. For instance, TRKA mainly binds to NGF as well as NT-7/6 [10], while

TRKB binds to BDNF and NT-4/5 [11], and TRKC specifically binds to NT-3 [12]. Fusion of an *NTRK* might cause the loss of form or function of the extracellular domain of the TRK protein, and ultimately lead to continuous activation and overexpression [13,14]. The activation of TRKs receptors will trigger downstream signal transduction pathways involving phosphatidylinositol 3 kinase (PI3K)/AKT and RAS/RAF, which are considered as a pan-cancer carcinogenic factor [15–17]. Considering that the fusion of TRKs usually results in the loss of the extracellular domain, monoclonal antibodies will not be able to target the mutated TRK protein. Therefore, small molecule inhibitors may be the only key to target TRKs to treat tumors.

A few potent TRKs inhibitors have been reported, including type I, type II, and type III inhibitors, based on their site of binding to TRKs. Among them, **AZ-23** (**1**) is a pan-TRKs inhibitor with 2,4-diaminopyrimidine core, which was active against TRKA ($IC_{50} = 2$ nM) and TRKB ($IC_{50} = 8$ nM) [18]. In addition, the researchers also obtained the co-crystal of **AZ-23** and TRKA (PDB ID 4AOJ, 2.75 Å), revealing the binding mode of this type of inhibitors and TRKs, laying the foundation for the follow-up study of further works [19]. **Entrectinib** (**2**) is a multi-target kinases inhibitor which

* Corresponding author.

E-mail address: medchemzhao@163.com (D. Zhao).

was developed by Roche and approved by the FDA on August 15, 2019. It has presented robust suppressive activity on ALK ($IC_{50} = 12$ nM), ROS1 ($IC_{50} = 7$ nM), and all subtypes of TRKs (IC_{50} values for TRKA/B/C were 1 nM, 3 nM, and 5 nM, respectively) [20,21]. Most recently, Ding et al. identified a series compounds with 1*H*-indazole core as type I TRKs inhibitors (**3**). Compound **3** had activity on TRKA/B/C with IC_{50} values of 1.6 nM, 2.9 nM, and 2.0 nM, respectively. Moreover, **3** also exhibited excellent selectivity over a large kinases panel [22]. **Larotrectinib** (**4**) was another approved by FDA for treatment cancers containing *NTRKs* fusion, regardless of cancer types [23–25]. **PF-06273340** (**5**) is a type II inhibitor for TRKs, which was reported by Pfizer and in Phase I clinical trials currently. Su and his colleagues discovered 9*H*-fluorene derivatives (**6**) as a type III inhibitor that bond to the juxta-membrane (JM) domain of TRKA. Compound **6** displayed TRKA activity and >250-fold selectivity over TRKB and TRKC (TRKA $IC_{50} = 99$ nM, TRKB $IC_{50} > 8100$ nM, TRKC $IC_{50} = 2500$ nM) (Fig. 1) [26].

To analyze the structure of several type I inhibitors against TRKs (Compound **1** to **3**), it is not difficult to find that they have similar structural features and binding modes: An aminopyrazole fragment binds to the hinge of the kinases, and an aryl fragment extends into the hydrophobic pocket adjacent to the DFG motif (see Fig. 1). Based on above analysis and with the aid of computer-aided drug design (CADD), we constructed a ligand-based pharmacophore model of competitive inhibitors of TRKs. Common features of this pharmacophore model include: One hydrogen bond donor and two hydrogen bond acceptors form interactions with the hinge (shown as blue in Fig. 2); A benzene or pyridine ring which is substituted by fluorine atoms linked by the flexible chain extends towards a hydrophobic pocket composed of Asn-655, Cys-656, Gly-667, and so on (shown as red in Fig. 2); The other two hydrophobic centers form hydrophobic interactions with Phe-589, the gatekeeper residue, and Leu-516 (shown as red in Fig. 2). Then, for the development of novel type I TRKs inhibitors, we employed scaffold hopping strategy to design and synthesize a tetrahydropyrrolo derivative **17a**, which possesses all the aforementioned pharmacophore characteristics

(shown as different colors in Fig. 2), and aligns well with **Entrectinib** in docking studies. The *in vitro* kinase assays showed that compound **17a** was weak active against TRKA ($IC_{50} = 1.24$ μ M). Then, compound **7** (**17h**, $IC_{50} = 0.47$ μ M) with stronger inhibitory activity than **17a** was discovered in hit to lead stage. Meanwhile, the importance of the fluorine atom in contribution to activity was realized. Therefore, we carried out the next structural modification around the fluorine atom. With the **17i** ($IC_{50} = 0.19$ μ M) and **17m** ($IC_{50} = 0.20$ μ M) were obtained, furthermore optimization and structure-activity relationship (SAR) study were conducted, which led to identification of a potent and selective TRKs inhibitor **8** (**19m**, $IC_{50} = 0.017$ μ M). Herein, based on the above strategy, a series of tetrahydropyrrolo[3,4-*c*]pyrazol derivatives were reported including the design, synthesis and biological evaluation of them. And finally, a more accurate pharmacophore model was given to try to help researchers to find selective type I TRKs inhibitors more efficiently.

2. Results and discussion

2.1. Chemistry

Target compounds **17a** - **17v** and **19a** - **19s** were synthesized in a few steps from a key intermediate **14**, a tetrahydropyrrolo[3,4-*c*]pyrazol core protected with Boc. The key intermediate **14** was prepared by a previously reported synthetic route, which was optimized moderately [27]. The amino acid **10** was prepared by utilizing a Michael addition reaction of 2-amino-2-methylpropanoic acid (**9**) and acrylonitrile. The amino group of **10** was then protected as a Boc carbamate (**11**). Intermediate **11** was reacted with iodomethane to yield methyl ester **12**. Compound **13** was synthesized by the cyclization of **12** under basic conditions. Finally, treatment of ketonitrile **13** with hydrazine under acetic acid conditions, afforded the key intermediate **14**.

For the synthesis of target compounds **17a** - **17v**, *N* atom located at pyrazol ring of the key intermediate **14** was selectivity protected by ethylcarbonyl chloride (**15**), followed by the condensation

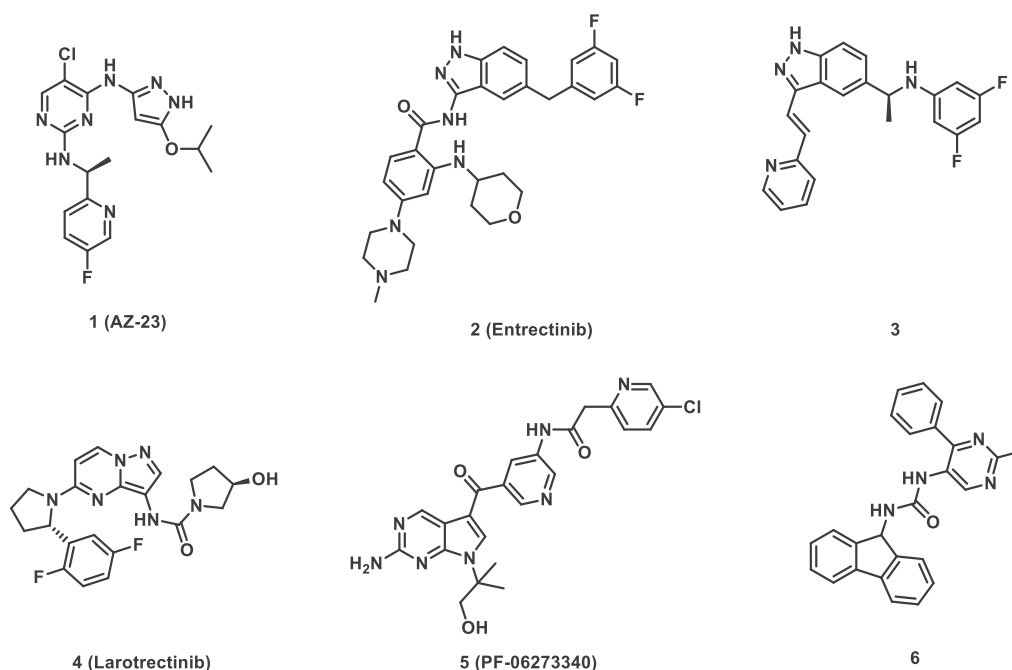


Fig. 1. Structures of potent TRK inhibitors.

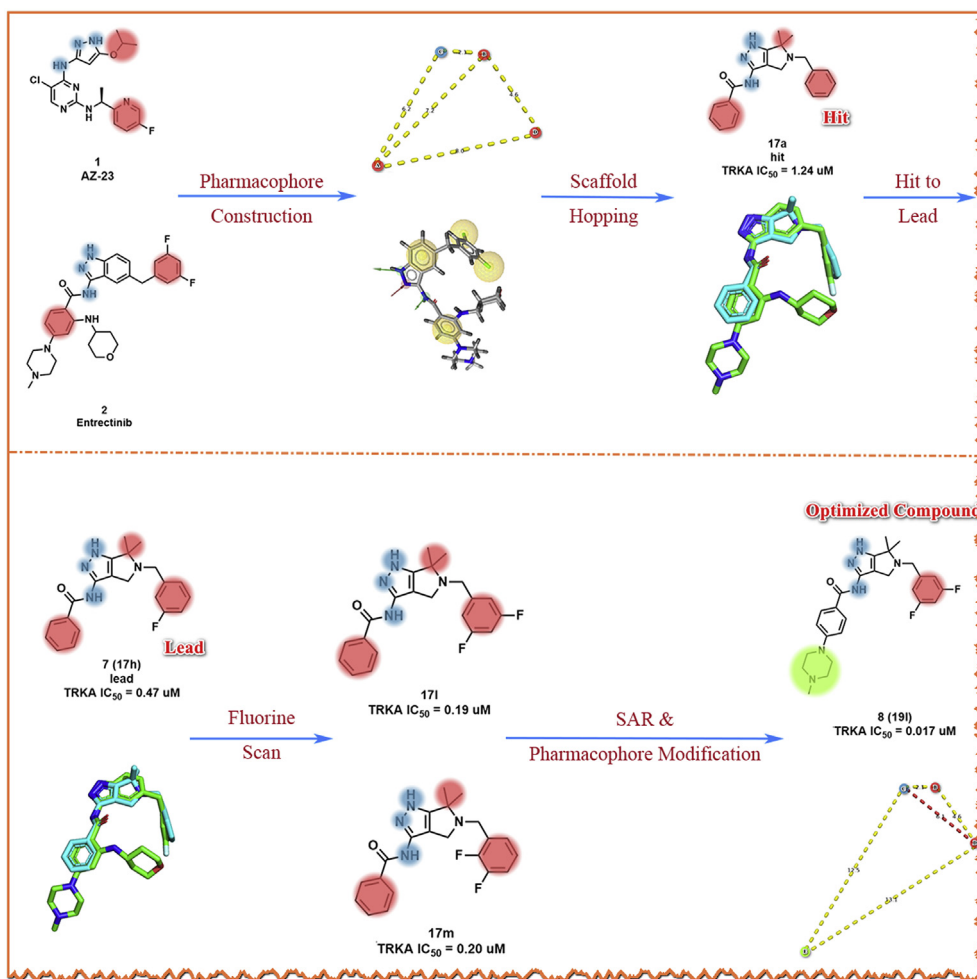


Fig. 2. Design and modification strategies of novel and selective TRKs inhibitors.

reaction with benzoyl chloride obtained intermediate **16**, which could be separated by recrystallization in a moderate quantity (>10 g) due to its smaller polarity. Then, the Boc group of **16** was cleaved to give an amine, which subsequently nucleophilic attacked on various substituted benzyl bromide, and finally deprotection with DIPEA to obtain the corresponding compounds **17a** - **17v** for one-pot.

Compounds **19a** - **19s** were synthesized according to the protocol described in the lower part of Scheme 1. Treatment of the key intermediate **14** with different chloride prepared by corresponding benzoic acid gave a mixture of compounds with mono-acylation (**18a** - **18t**) and bis-acylation, then the acylation at the pyrazol ring was removed by basic conditions to convert the bis-acylated compounds to mono-acylated compounds (**18a** - **18t**). Deprotection of **18a** - **18t**, followed by substitution reactions, which was similar to the preparation of **17a** - **17v**, obtained target compounds **19a** - **19s**.

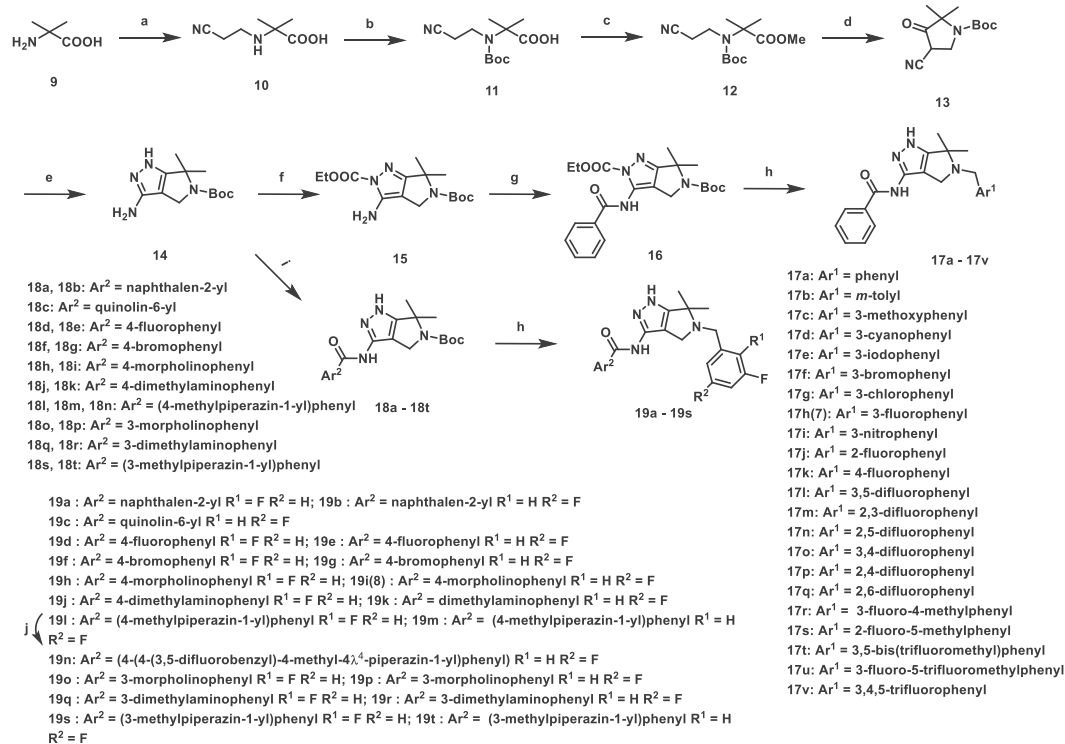
2.2. Target compounds design and in vitro activity against TRKs kinase

The *in vitro* inhibitory activity against TRKs of the novel synthesized compounds were evaluated by using the homogeneous time-resolved fluorescence (HTRF) assays, and **Larotrectinib** (**4**) was involved as a comparison. Under our experimental conditions, **Larotrectinib** exhibited suppressive activity on TRKA, TRKB, and

TRKC with IC_{50} values of 3.4 nM, 4.7 nM, and 0.9 nM, respectively, which was similar to previously outlined data [22].

According to the constructed pharmacophore model, we first designed and synthesized the compound **17a** ($IC_{50} = 1.24 \mu M$) as a hit. The docking study indicated that aminopyrazol moiety in **17a** formed three key hydrogen bonds with Glu-590 and Met-592 in hinge region of the TRKA. The tetrahydropyrrolo ring occupying the adenine region, and two methyls in the ring formed hydrophobic interactions with gatekeeper Phe-589 and neighbouring residues. The benzyl moiety located downward in a hydrophobic pocket, and generated anion- π interactions with Asp-668 from DFG motif (Fig. 3A).

Guided by docking study, we found that the hydrophobic cavity adjacent to the DFG motif was not occupied completely, suggested that introducing a suitable substituent at the *meta*-position of the benzyl moiety in **17a** could further occupy the cavity and might improve the inhibitory activity of compounds (Fig. 3B). Therefore, we synthesized and tested the inhibitory activity of analogues **17b** to **17i**, and the results were shown in Table 1. Compared to compound **17a**, introduction of a bulky substituent (**17b** to **17f**) at the 3-position of the benzyl moiety resulted no significant improve in activity, indicating that the cavity is limited in size. While analogue **17g** ($IC_{50} = 0.67 \mu M$) displayed better potency than **17a**. Furthermore, switching chlorine atom to fluorine atom (**17h**) led to further increase in activity ($IC_{50} = 0.47 \mu M$). The potency improve of **17h** might be explained by the fluorine atom formed halogen



Scheme 1. Synthesis of compounds **17a - 17v** and **19a - 19s**. Reagents and conditions: (a) acrylonitrile, NaOH (aq), r.t., 24 h; (b) (Boc)₂O, TMAH, TEA, DMAP, CH₃CN, 40 °C, 10 h; (c) MeI, K₂CO₃, DMF, 40 °C, 2 h; (d) NaH, dry 1,4-dioxane, reflux, 3 h; (e) NH₂NH₂, AcOH, EtOH, reflux, 9 h; (f) Ethylcarbamoyl chloride, DIPEA, dry THF, -40 °C, 2 h; (g) PhCOCl, DIPEA, dry DCM, 30 °C, overnight; (h) i. TFA, DCM, r.t., 1 h; ii. appropriate benzyl bromide, DIPEA, MeOH, 45 °C, 3 h; (i) i. appropriate chloride, DIPEA, dry DCM, -20 °C, 2 h; ii. TEA, MeOH, reflux, 2 h; (j) 1-(bromomethyl)-3,5-difluorobenzene, DIPEA, MeOH, 45 °C, 8 h.

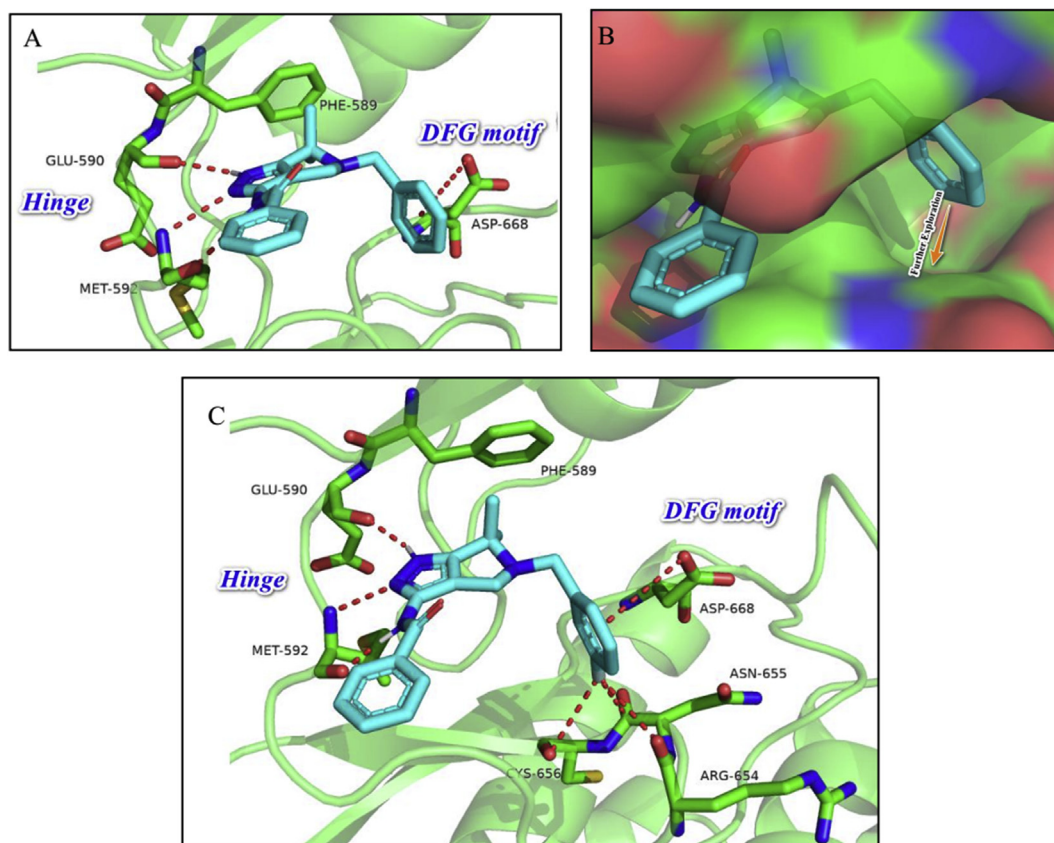


Fig. 3. Molecular docking of **17a** (A and B) and **17h** (C) in the ATP-binding site of TRKA. The kinase is depicted in green ribbons, and interactions are illustrated with red dashed lines.

Table 1
In vitro TRKA kinase inhibitory activity of the **17a** to **17i**^a.

Entry	R ³	TRKA IC ₅₀ (μM)	Entry	R ³	TRKA IC ₅₀ (μM)
17a	H	1.24	17f	Br	0.94
17b	Me	1.10	17g	Cl	0.67
17c	Me	1.12	17h(7)	F	0.47
17d	CN	0.98	17i	NO ₂	0.60
17e	I	1.36	Larotrectinib	—	0.0034

^a The IC₅₀ values are shown as the mean (μM) values from two separate experiments.

interactions with Cys-656, Arg-654, and Asn-644 (Fig. 3C). Compound **17h** (**7**) with moderate potency and minor molecular weight, was an acceptable lead compound for further optimization.

Since the performance of the fluorine atom in hit to lead stage, we focused our attention on introducing more fluorine atoms or changing the position of fluorine atoms on the benzyl group of the lead compound **17i**. (Table 2). The *in vitro* kinase assays with analogue **17j**, **17k**, and **17h** was showing that the analogue **17j** with *ortho*-position fluorine and **17h** with *meta*-position fluorine exhibited approximately same potency, while the 4-position of fluorine (**17k**) was not tolerated (IC₅₀ = 1.18 μM). Incorporation of another fluorine atom in benzyl of **17k** afforded analogue **17o** and **17p**, and their potency were weaker than the lead, yet (IC₅₀ = 0.68 μM, and 2.32 μM, respectively). The other analogues with difluorophenyl fragment (**17l**, **17m**, **17n**, and **17q**) displayed moderate inhibitory activity. In particular, the 3,5-difluorophenyl and 2,3-difluorophenyl at Ar¹ (**17l** and **17m**) exhibited the best

Table 2
In vitro TRKA kinase inhibitory activity of the **17j** to **17v**^a.

Entry	Ar ¹	TRKA IC ₅₀ (uM)	Entry	Ar ¹	TRKA IC ₅₀ (uM)
17j		0.45	17q		0.52
17k		1.18	17r		0.94
17l		0.19	17s		0.88
17m		0.20	17t		16.36
17n		0.48	17u		1.00
17o		0.68	17v		6.96
17p		2.32	17h(7)		0.47
	Larotrectinib	—			0.0034

^a The IC₅₀ values are shown as the mean (uM) values from two separate experiments.

activity to TRKA (IC₅₀ = 0.19 μM, and 0.20 μM, respectively).

For further exploring the structure-activity relationships (SAR), we tried to replace fluorine atoms with a larger methyl group provided **17r** and **17s**, with decreased enzyme activity (IC₅₀ = 0.94 μM, and 0.88 μM, respectively). Replacement of the fluorine atom with one or two trifluoromethyls (**17u**, **17t**) also led to obvious activity loss against TRKA (IC₅₀ = 1.00 μM, and 16.36 μM, respectively). These results might confirm that the cavity is limited in size. Analogue **17v** also exhibited significant potency loss (IC₅₀ = 6.96 μM), which might be explained by adverse effects of *para*-position fluorine atom. In conclude, Compound **17l** and **17m** with the best potency of them were chosen for further optimization.

We next focused on the Ar¹ moieties by fixing benzyl moieties with 2,3-difluorophenyl and 3,5-difluorophenyl (Table 3). *In vitro* kinase assays with analogues **19a** to **19g** indicated that hydrophobic substituents in Ar¹ were detrimental to activity. Based on the above results, we then chose to introduce some hydrophilic fragments on the benzene ring (**19h** to **19m**). All of these compounds exhibited stronger inhibitory activity than **17l** and **17m**, which were preferred compounds in last round of structural modification.

Furthermore, using the 3,5-difluorobenzyl moiety to ionize analogue **19m** (IC₅₀ = 0.017 μM) gave quaternary ammonium salt **19n** (IC₅₀ = 0.095 μM), which displayed measurable decreases in potency. Changing the position of substituent of **19h** to **19m** from *para* to *meta* provided analogues **19o** to **19t**, without improving enzyme activity, yet. Finally, we selected analogues **19h**, **19i**, **19l**, **19m**, **19p** and **19t** because of their stronger inhibitory activity, to test activity on the enzyme level of TRKB and TRKC (Table 4). The results showed that all the analogues were pan-TRK inhibitor, as their significant inhibitory effect on each subtype of TRKs.

2.3. Antiproliferative activity

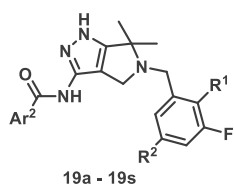
Above six analogues (**19h**, **19i**, **19l**, **19m**, **19p** and **19t**) were further evaluated for *in vitro* anticancer screening. Their IC₅₀ values against Km-12 cells line which harbors TRKA rearrangement was tested and listed in Table 5. Meanwhile, the lung cancer cells line A549 and the liver epithelial cells line THLE-2, neither of them have TRKA gene fusion, had also been tested to evaluate potential off-target effects of TRKs inhibitors. As shown in Table 5, compared with A549 and THLE-2, analogues **19h**, **19i**, **19l** and **19m** exhibited more than 200-fold selectivity to Km-12. This means that the risk of off-target effects of these compounds may be low. In addition, these compounds also showed potent antiproliferative effects on Km-12 cell lines. Among them, analogue **19m** has the strongest activity (IC₅₀ = 0.082 μM) and selectivity (Km-12 vs A549, 882-fold; Km-12 vs THLE-2, >1220-fold). As a result, analogue **19m** was selected for further research.

2.4. Effects of analogue **19m** on cell apoptosis

The ability of analogue **19m** to induce apoptosis of Km-12 cells was tested by flow cytometry. Analogue **19m** strongly induced apoptosis in a concentration-dependent manner with apoptotic rates of 29.44%, 36.38% and 69.79% at concentrations of 0.0625 μM, 0.125 μM and 0.25 μM, respectively. When the concentration was greater than 0.25 μM, with the further increase of the administration concentration, the compound had no significant effects on apoptosis (Fig. 4).

2.5. Effects of analogue **19m** on cell cycle

We further examined the effects of analogue **19m** on the cell cycle. With the increase in the concentration of administration, the

Table 3
In vitro TRKA kinase inhibitory activity of the **19a** to **19s**^a.


Entry	Ar ²	R ¹	R ²	TRKA IC ₅₀ (uM)
19a		F	H	0.46
19b		H	F	0.44
19c		H	F	0.18
19d		F	H	0.21
19e		H	F	0.35
19f		F	H	0.95
19g		H	F	0.71
19h		F	H	0.029
19i		H	F	0.014
19j		F	H	0.069
19k		H	F	0.096
19l		F	H	0.017
19m		H	F	0.017

Table 3 (continued)

Entry	Ar ²	R ¹	R ²	TRKA IC ₅₀ (uM)
19n		H	F	0.095
19o		F	H	0.27
19p		H	F	0.12
19q		F	H	0.42
19r		H	F	0.27
19s		F	H	0.21
19t		H	F	0.15
Larotrectinib	—	—	—	0.0034

^a The IC₅₀ values are shown as the mean (μM) values from two separate experiments.

Table 4
In vitro TRKs kinase inhibitory activity of compounds.^a

Entry	TRKA IC ₅₀ (uM)	TRKB IC ₅₀ (uM)	TRKC IC ₅₀ (uM)
19h	0.029	0.035	0.010
19i	0.014	0.027	0.0090
19l	0.017	0.023	0.013
19m	0.017	0.028	0.011
19p	0.12	0.17	0.075
19t	0.15	0.19	0.10
Larotrectinib	0.0013	0.0047	0.0010

^a The IC₅₀ values are shown as the mean (μM) values from two separate experiments.

G1 phase ratio of the Km-12 cells line gradually increased, the S phase ratio gradually decreased, and finally leveled off at 0.25 μM,

Table 5
Relative IC₅₀ (μM) values and selectivity for selected compounds against Km-12, A549 and THLE-2 cells.

Entry	IC ₅₀ ^a			Km-12 select.index ^b	
	Km-12 (μM)	A549 (μM)	THLE-2 (μM)	Km-12 vs A549	Km-12 vs THLE-2
19h	0.146 ± 0.015	88.53 ± 1.57	49.48 ± 1.48	606x	339x
19i	0.211 ± 0.077	>100	>100	>474x	>474x
19l	0.216 ± 0.098	64.18 ± 2.14	>100	297x	>463x
19m	0.082 ± 0.008	72.29 ± 5.06	>100	882x	>1220x
19p	>1	—	—	—	—
19t	>1	—	—	—	—

^a IC₅₀: concentration of the compound (μM) producing 50% cell growth inhibition after 72 h of drug exposure, as determined by the CCK-8 assay.

^b A549 IC₅₀ or THLE-2 IC₅₀/Km-12 IC₅₀, x = fold.

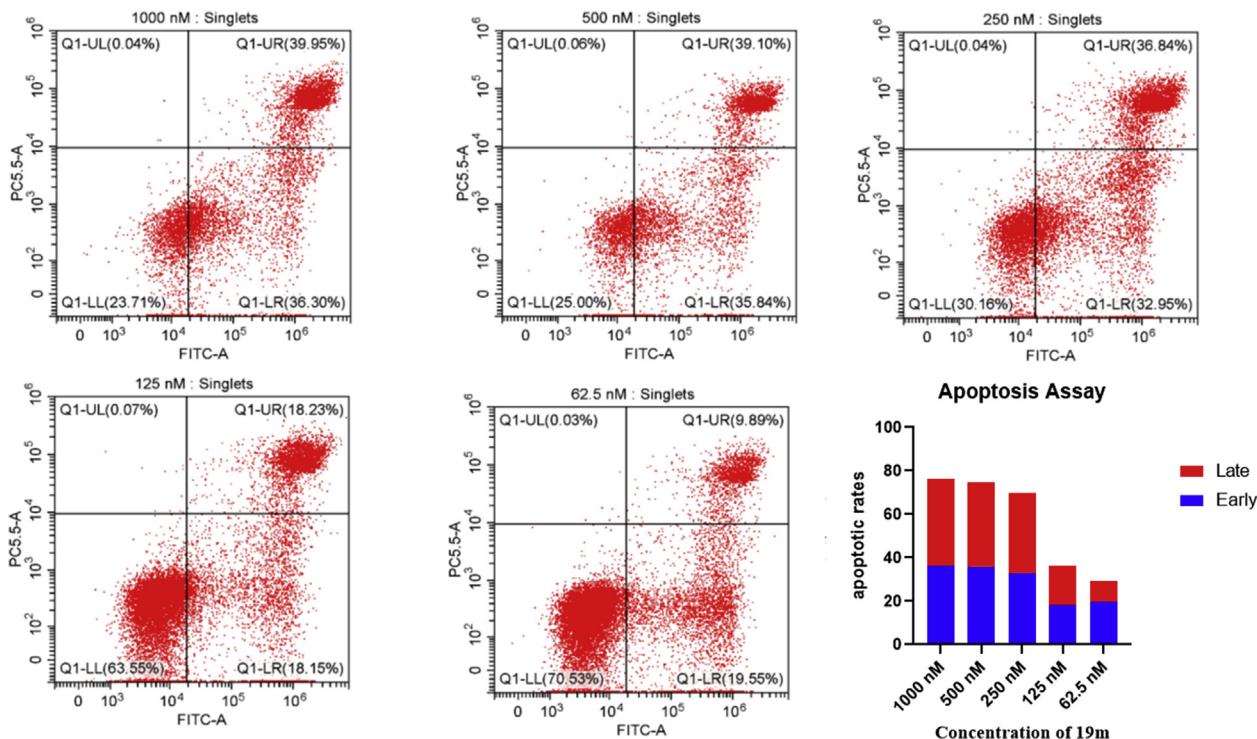


Fig. 4. Effects of analogue **19m** on Km-12 cells apoptosis.

which was compatible with the results of the apoptosis test. These data demonstrated that analogue **19m** could effectively lead to G1/S phase arrest in Km-12 cells (Fig. 5).

2.6. Kinase selectivity profile

In order to further evaluate the selectivity of this series, the potent analogue **19m** was profiled against a panel of 28 kinases at a concentration of 1.0 μM, and the percent inhibition values were shown in Table 6 and Fig. 6. The analogue **19m** had good kinase selectivity, with only TRKs and ALK producing greater than 80% inhibition (red columns in Fig. 6). Four kinases were inhibited by **19m** to an extent 40%–80% (yellow columns in Fig. 6), and the other kinases were inhibited less than 40% (green columns in Fig. 6). These above experimental results were consistent with the cell antiproliferative test results.

2.7. In vitro metabolic stability and CYPs inhibition

Next, the *in vitro* plasma stability and liver microsomal stability of analogue **19m** were also evaluated. As shown in Table 7, analogue

19m possessed favorable plasma stability with $t_{1/2} > 4.8$ h. Liver microsomal experiments displayed that **19m** had relatively acceptable metabolic stability. Without NADPH, the recovery rate was 90%, which indicated that analogue **19m** was metabolized through the NADPH-dependent oxidation pathway (Table 8).

Analogue **19m** was then evaluated with a panel of cytochrome P450 isoforms (1A2, 2C9, 2C19, 2D6 and 3A4). None of them were obviously inhibited by **19m** at a concentration of 10.0 μM, indicating minimal drug-drug potential with compounds cleared predominantly via these metabolic pathways (Table 9).

2.8. In vivo pharmacokinetics properties

Then, the pharmacokinetic profile in rat for analogue **19m** was evaluated and the corresponding data were showed on Table 10. The rats were treated with **19m** at the dose of 3 mg/kg or 1 mg/kg which depended on the different way of administration (p.o. or i.v.). Analogue **19m** exhibited moderate half-time of 1.89 ± 0.06 h for p.o. and 1.51 ± 0.36 h for i.v. A good area under the curve was detected, whether the way of administration was p.o. or i.v. Analogue **19m** also had a low plasma clearance of 8.08 ± 1.00 mL/min/kg and a

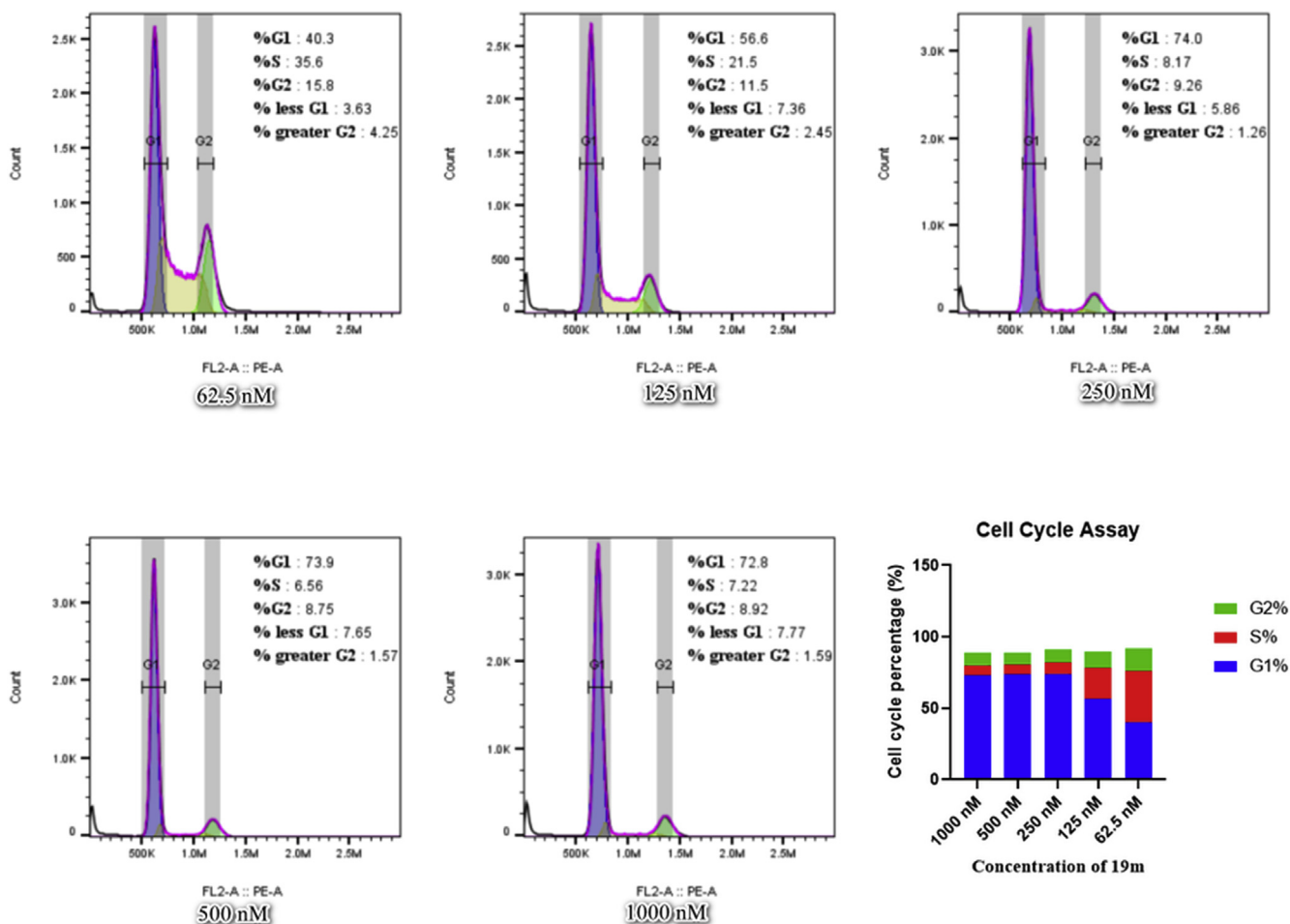


Fig. 5. Effects of analogue **19m** on Km-12 cells cycle.

Table 6

Kinase selectivity profile of analogue **19m**^a.

Kinases	%inhibition @1.0 μ M	Kinases	%inhibition @1.0 μ M	Kinases	%inhibition @1.0 μ M	Kinases	%inhibition @1.0 μ M
TRKA	102	FAK	51	MEK	8	CDK2	3
TRKB	100	BTK	35	TBK1	7	PRKCA	3
TRKC	99	FLT3	31	cMet	6	AKT1	2
ALK	82	MELK	22	EGFR	4	mTOR	1
JAK2	76	RAF1	11	PAK4	4	PLK4	0
FGFR1	60	Aurora A	11	BRAF	3	ERK1	0
AMPK	53	ROS1	10	PAK1	3	PIM1	0

Profiling Service from Life Technologies. The results represent the mean of three independent experiments performed in triplicate.

^a Selectivity profile of analogue **19m** measured at a concentration of 1.0 μ M in a panel of 28 kinase generated with the SelectScreen®.

good volume of distribution (892 ± 150 mL/kg). The oral bioavailability was 44.3%, which was an acceptable result that will be improved in further research.

2.9. Binding mode and pharmacophore model analysis

To investigate the interaction mode of analogue **19m**, a docking study of this analogue in the ATP-binding site of TRKA (PDB entry: 5 kvt) was performed. The best predicted binding mode is shown in Fig. 7, and has a calculated binding energy of -12.55 kcal/mol. As shown in Fig. 7, the aminopyrazole fragment forms three hydrogen bonds to the backbone carbonyl oxygen of Glu-590, the NH and carbonyl oxygen of Met-592 in the hinge region. Further stabilization may be achieved through the hydrophobic interaction of

tetrahydropyrrolo scaffold with the hydrophobic side chains of gatekeeper Phe-589. Meanwhile, the fluorine atom on benzyl motif served as a fluorine bond donor for Asn-655 and Gly-667. In addition, the benzyl moiety also interacts with Asp-668 of the DFG motif via anion- π interaction, and the *N*-methylpiperazine fragment towards the solvent region.

Through the above analysis of the binding mode and the test results of *in vitro* enzyme activity, we abstracted the structural characteristics of the inhibitor into four pharmacophore characteristics. Different from the pharmacophore model that we relied on calculation at the beginning, the new pharmacophore model has been revised by experimental results and thus become more reliable. The new pharmacophore model includes a hydrogen bond center (C, blue in Fig. 8), two hydrophobic centers (B and D, red in

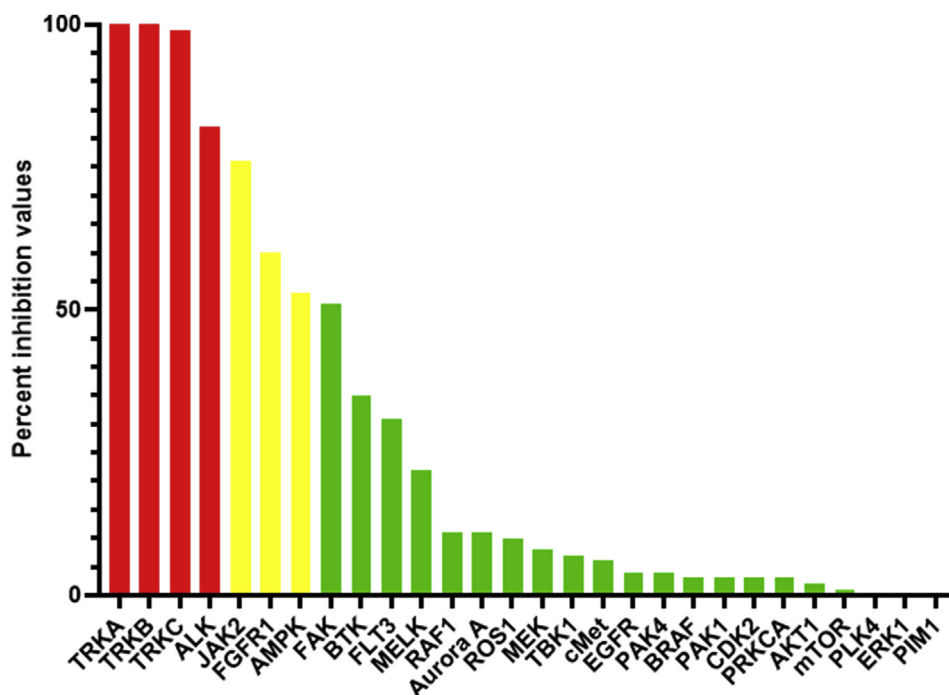


Fig. 6. Selectivity profile of analogue **19m** measured at a concentration of 1.0 μM in a pannel of 28 kinases (red columns denote >80%, yellow columns denote between 40% and 80%, and green columns denote <40%).

Table 7
Plasma stability of analogue **19m**.

Time Point (min)	0	10	30	60	120
Remaining (%)	100.0	96.8	95.7	99.2	100.7
$T_{1/2}$ (min)	>289.1				

Fig. 8), and a hydrophilic center (E, green in **Fig. 8**), the four of which are cross-linked to form a non-strict isosceles triangle. Among them, the hydrogen bond center C used to form hydrogen bonds with hinge region and the hydrophobic center D with fluorine atoms are two most critical pharmacophores, which play a key role in maintaining the potent activity of the inhibitor. In addition, in the study of the structure-activity relationship, we found that introduction of a hydrophilic center E can further increase the activity of inhibitors, while the benzene ring connected to the center E may only serve as a backbone support. Because of this, we replaced the hydrophobic center A corresponding to the benzoyl group in the original pharmacophore model with the hydrophilic center E, which is also the core difference between the new and old pharmacophore models. We hope that this renew and more accurate pharmacophore model can help researchers more efficiently discover selective TRKs inhibitors with a novel parent scaffold. The new pharmacophore-based drug design of TRK inhibitors are ongoing by us, and will be reported in due course.

Table 8
Liver microsomal stability of analogue **19m**.

Parameters	R^2	$T_{1/2}$	$CL_{\text{int(mic)}}$ ($\mu\text{L}/\text{min}/\text{mg}$)	$CL_{\text{int(liver)}}$ ($\mu\text{L}/\text{min}/\text{mg}$)	Remaining (%) ($T = 60 \text{ min}$)	Remaining (%) (NCF ^a , $T = 60 \text{ min}$)
In human	0.99	29.6	46.8	42.1	22.4	90.9

^a NCF: abbreviation of no co-factor. No NADPH was added to NCF samples (replaced by buffer) during the 60 min incubation.

Table 9
Cytochrome P450 inhibition of analogue **19m**^a.

Isozyme	CYP1A2	CYP2C9	CYP2C19	CYP2D6	CYP3A4
Inhibition at 10 μM (%)	12.9	16.0	11.5	0.0	6.4

^a Assay were performed in pooled human liver microsomes.

3. Conclusion

By analyzing the structural characteristics and binding mode of type I TRK inhibitors, we first constructed a rough pharmacophore model. Under the guidance of the early pharmacophore, a series of novel tetrahydropyrrolo [3,4-c] pyrazol derivatives were obtained using scaffold hopping strategy. One of the best compounds, **19m** (TRKA $IC_{50} = 0.017 \mu\text{M}$, TRKB $IC_{50} = 0.028 \mu\text{M}$, TRKC $IC_{50} = 0.011 \mu\text{M}$), showed potent anti-proliferative activity on Km-12 cell lines ($IC_{50} = 0.082 \pm 0.008 \mu\text{M}$) and remarkable selectivity between TRK-dependent cell lines and TRK-independent cell lines (>800-fold). Compound **19m** strongly induced apoptosis and G1/S phase arrest on Km-12 cell lines. The kinase selectivity evaluation displayed that compound **19m** has good kinase selectivity. In addition, compound **19m** possesses favorable plasma stability, moderate liver microsomal stability, and low CYPs inhibition *in vitro*, and good ADME properties *in vivo*. Taken together, compound **19m** may serve as a lead compound for drug discovery to treat cancer caused by *NTRK* gene fusion. Moreover, during the research process, we delved into the structure-activity relationship

was adjusted to 3 with concentrated hydrochloric acid under ice bath, and then absolute ethanol (50 mL) was added. The suspension was stirred for an additional 15 min, and filtered under reduced pressure to obtain a white solid in 82% yield, which was used in the next step without additional purification.

4.1.2. 2-[(*tert*-butoxycarbonyl)(2-cyanoethyl)amino]-2-methylpropanoic acid (**11**)

To solution of **10** (62.10 g, 0.40 mol) and tetramethylammonium hydroxide (79.27 g, 0.44 mol) in acetonitrile (500 mL) were carefully added the mixture of di-*tert*-butyl dicarbonate (216.95 g, 0.99 mol), triethylamine (138.17 mL, 0.99 mol) and 4-dimethylaminopyridine (12.14 g, 0.10 mol) in acetonitrile (500 mL) at 0 °C. The mixture was heated to 40 °C for 10 h, and then cooled to room temperature. The solvent was removed. The oil residue was subsequently dissolved in water (500 mL), and washed with ethyl acetate (250 mL × 3). The pH of aqueous layer was adjusted to 4 with citric acid, extracted with ethyl acetate (250 mL × 3), and washed with brine (250 mL × 3). The organic layer was dried over anhydrous sodium sulfate and concentrated to give a orange oil in 53% yield, which was used in the next step without additional purification.

4.1.3. Methyl 2-[(*tert*-butoxycarbonyl)(2-cyanoethyl)amino]-2-methylpropanoate (**12**)

A well stirred mixture of **11** (54.01 g, 0.21 mol), potassium carbonate (87.38 g, 0.63 mol), and iodomethane (26.24 mL, 0.42 mol) in *N,N*-dimethylformamide (400 mL) was heated to 40 °C for 2 h. The suspension was poured into ice saturated ammonium chloride solution (2000 mL), extracted with ethyl acetate (500 mL × 3) and washed with brine (500 mL × 3). The combined organic fractions were dried over anhydrous sodium sulfate, filtered, and evaporated to dryness to obtain crude product as a yellow oil in 94% yield, which was used in the next step without further purification.

4.1.4. *Tert*-butyl 4-cyano-2,2-dimethyl-3-oxopyrrolidine-1-carboxylate (**13**)

A solution of **12** (53.55 g, 0.20 mol) in 1,4-dioxane (400 mL) was cooled to 0 °C, treated with 60% sodium hydride carefully, then heated at reflux for 3 h. The reaction mixture was cooled to room temperature and cautiously quenched with water (9 mL). The solvent was removed, and the resulting oil was redissolved in water (200 mL). The pH of the aqueous layer was adjusted to 4 with citric acid, extracted with ethyl acetate (200 mL × 3), washed with brine (200 mL × 3), and concentrated to give a yellow oil in 93% yield, which was used in the next step without further purification.

4.1.5. *tert*-butyl-3-amino-6,6-dimethyl-3a,4,6,6a-tetrahydropyrrolo[3,4-*c*]pyrazole-5(1*H*)-carboxylate (**14**)

To solution of **13** (43.90 g, 0.18 mol) and acetic acid (84.92 mL, 1.47 mol) in absolute ethanol (500 mL) were added 80% hydrazine hydrate (57.63 mL, 0.92 mol), then heated at reflux for 9 h. The reaction mixture was cooled to room temperature, concentrated, and redissolved in water (300 mL). The pH of aqueous layer was adjusted to 9 with saturated sodium carbonate solution, extracted with ethyl acetate (150 mL × 3), and washed with brine (150 mL × 3). The combined organic layers were dried over anhydrous sodium sulfate, and filtered. The filtrate was concentrated to yield a yellow oil in 75% yield, which was used in the next step without further purification.

4.1.6. 5-(*tert*-butyl) 2-ethyl 3-amino-6,6-dimethylpyrrolo[3,4-*c*]pyrazole-2,5(4*H*,6*H*)-dicarboxylate (**15**)

A solution of **14** (20.00 g, 0.14 mol) and *N,N*-disopropylethylamine (48.13 mL, 0.28 mol) in anhydrous tetrahydrofuran (300 mL)

were cooled to −40 °C and then a solution of ethyl carbonochloridate (11.84 mL, 0.12 mol) in anhydrous tetrahydrofuran (300 mL) was added drop wise. After the TLC showed that majority of the starting material was converted to the product, the tetrahydrofuran was removed, and oil residue was dissolved in dichloromethane (300 mL). The organic layer was washed with water (150 mL × 3), and evaporated to dryness to provide a yellow. Then ethyl ether (80 mL) was added to the residue and the resulting slurry was stirred at room temperature for 2 h, filtered and the filter cake was the target product as a white solid. Yield, 42%.

4.1.7. 5-(*tert*-butyl)2-ethyl3-benzamido-6,6-dimethylpyrrolo[3,4-*c*]pyrazole-2,5(4*H*,6*H*)-dicarboxylate (**16**)

A solution of **15** (18.82 g, 0.058 mol) in anhydrous dichloromethane (200 mL) was added *N,N*-disopropylethylamine (20.22 mL, 0.12 mol). The solution was cooled to 0 °C, and then a solution of benzoyl chloride (7.36 mL, 0.064 mol) in anhydrous dichloromethane (100 mL) was added dropwise. The reaction mixture was heated to 30 °C for overnight. The solvent was removed, and then recrystallized with petroleum ether to give the pure product as a white solid. Yield, 84%. ¹H NMR (600 MHz, DMSO-*d*₆) δ 10.85 (s, 1H), 7.92 (d, *J* = 7.7 Hz, 2H), 7.69 (t, *J* = 7.4 Hz, 1H), 7.61 (t, *J* = 6.9 Hz, 2H), 4.55 (d, *J* = 13.6 Hz, 2H), 4.46 (q, *J* = 7.1 Hz, 2H), 1.62 (2s, 6H, rotamers.), 1.47 (2s, 9H, rotamers.), 1.37 (t, *J* = 7.1 Hz, 3H).

4.1.8. General procedure for the synthesis of target compounds **17a** - **17v**

A mixture of **16** (0.20 g, 0.47 mmol) and trifluoroacetic acid (0.50 mL) in dichloromethane (1.00 mL) were stirred at room temperature for 1 h. The reaction mixture was evaporated to dryness, redissolved in methanol (2 mL), *N,N*-disopropylethylamine was added to adjust the pH of mixture to 10, then treated with corresponding benzyl bromide (2.35 mmol), and stirred at 45 °C for an additional 3 h. The reaction was subsequently evaporated to dryness, redissolved in ethyl acetate (70 mL), and washed with water (35 mL × 3). The crude organic was concentrated and purified with silica chromatography (1% Methanol/Dichloromethane) gave the title compounds **17a** - **17v** in moderate yield.

4.1.8.1. *N*-(5-benzyl-6,6-dimethyl-1,4,5,6-tetrahydropyrrolo[3,4-*c*]pyrazol-3-yl)benzamide (**17a**). White solid. Yield: 51%. m.p. 190.4–191.1 °C ¹H NMR (600 MHz, DMSO-*d*₆) δ 12.24 (s, 1H), 10.66 (s, 1H), 7.91 (d, *J* = 7.7 Hz, 2H), 7.62–7.40 (m, 3H), 7.38 (t, *J* = 5.3 Hz, 2H), 7.33 (q, *J* = 6.8 Hz, 2H), 7.24 (q, *J* = 6.5 Hz, 1H), 3.78 (s, 2H), 3.64–3.46 (m, 2H), 1.37 (s, 6H). ¹³C NMR (151 MHz, DMSO-*d*₆) δ 164.49, 140.76, 132.14, 128.82, 128.79, 128.66, 128.16, 127.16, 59.78, 52.39, 40.54, 24.04. *R*_f = 0.075 (4% Methanol/Dichloromethane). HRMS (ESI, *m/z*) calcd for C₂₁H₂₂N₄O [M+H]⁺, 347.1872; found 347.1893.

4.1.8.2. *N*-[6,6-dimethyl-5-(3-methylbenzyl)-1,4,5,6-tetrahydropyrrolo[3,4-*c*]pyrazol-3-yl]benzamide (**17b**). White solid. Yield: 53%. m.p. 152.1–152.9 °C ¹H NMR (600 MHz, DMSO-*d*₆) δ 10.68 (s, 1H), 7.92 (d, *J* = 7.7 Hz, 2H), 7.54 (s, 1H), 7.47 (d, *J* = 8.4 Hz, 2H), 7.25–7.12 (m, 3H), 7.05 (d, *J* = 7.4 Hz, 1H), 3.74 (s, 2H), 3.56 (s, 2H), 2.30 (s, 3H), 1.36 (s, 6H). ¹³C NMR (151 MHz, DMSO-*d*₆) δ 164.49, 130.14, 129.39, 128.80, 128.54, 128.17, 127.83, 125.96, 59.74, 52.36, 40.54, 24.01, 21.53. *R*_f = 0.075 (4% Methanol/Dichloromethane). HRMS (ESI, *m/z*) calcd for C₂₂H₂₄N₄O [M+H]⁺, 361.2028; found 361.2043.

4.1.8.3. *N*-[5-(3-methoxybenzyl)-6,6-dimethyl-1,4,5,6-tetrahydropyrrolo[3,4-*c*]pyrazol-3-yl]benzamide (**17c**). White solid. Yield: 35%. m.p. 124.8–125.7 °C ¹H NMR (600 MHz, DMSO-*d*₆)

δ 10.69 (s, 1H), 7.92 (d, $J = 7.7$ Hz, 2H), 7.54 (d, $J = 8.2$ Hz, 1H), 7.46 (s, 2H), 7.24 (t, $J = 7.8$ Hz, 1H), 6.99–6.90 (m, 2H), 6.82–6.80 (m, 1H), 3.75 (s, 2H), 3.74 (s, 3H), 3.59 (s, 2H), 1.35 (s, 6H). $R_f = 0.075$ (4% Methanol/Dichloromethane). HRMS (ESI, m/z) calcd for $C_{22}H_{24}N_4O_2$ $[M+H]^+$, 377.1978; found 377.1983.

4.1.8.4. *N*-[5-(3-cyanobenzyl)-6,6-dimethyl-1,4,5,6-tetrahydropyrrolo[3,4-*c*]pyrazol-3-yl]benzamide (**17d**). White solid. Yield: 57%. m.p. 129.7–130.6 °C 1H NMR (600 MHz, DMSO- d_6) δ 12.27 (s, 1H), 10.70 (s, 1H), 7.92 (d, $J = 7.6$ Hz, 2H), 7.81 (s, 1H), 7.74 (t, $J = 8.2$ Hz, 2H), 7.61–7.37 (m, 4H), 3.85 (s, 2H), 3.68–3.47 (m, 2H), 1.37 (s, 6H). ^{13}C NMR (151 MHz, DMSO- d_6) δ 164.53, 142.77, 133.82, 132.17, 131.14, 130.00, 128.80, 128.17, 119.45, 111.70, 59.98, 51.58, 40.54, 24.14. $R_f = 0.20$ (4% Methanol/Dichloromethane). HRMS (ESI, m/z) calcd for $C_{22}H_{21}N_5O$ $[M+H]^+$, 372.1824; found 372.1829.

4.1.8.5. *N*-[5-(3-iodobenzyl)-6,6-dimethyl-1,4,5,6-tetrahydropyrrolo[3,4-*c*]pyrazol-3-yl]benzamide (**17e**). White solid. Yield: 55%. m.p. 212.8–213.9 °C 1H NMR (600 MHz, DMSO- d_6) δ 12.26 (s, 1H), 10.68 (s, 1H), 7.93 (s, 2H), 7.75 (t, $J = 1.7$ Hz, 1H), 7.61 (dt, $J = 7.8, 1.5$ Hz, 1H), 7.57–7.42 (m, 3H), 7.40 (dt, $J = 7.7, 1.3$ Hz, 1H), 7.15 (t, $J = 7.7$ Hz, 1H), 3.76 (s, 2H), 3.65–3.47 (m, 2H), 1.36 (s, 6H). ^{13}C NMR (151 MHz, DMSO- d_6) δ 164.52, 143.76, 137.22, 135.93, 130.94, 128.78, 128.30, 128.19, 95.31, 59.87, 51.70, 40.54, 24.10. $R_f = 0.19$ (4% Methanol/Dichloromethane). HRMS (ESI, m/z) calcd for $C_{21}H_{21}IN_4O$ $[M+H]^+$, 473.0838; found 473.0849.

4.1.8.6. *N*-[5-(3-bromobenzyl)-6,6-dimethyl-1,4,5,6-tetrahydropyrrolo[3,4-*c*]pyrazol-3-yl]benzamide (**17f**). White solid. Yield: 51%. m.p. 201.1–201.9 °C 1H NMR (600 MHz, DMSO- d_6) δ 12.26 (s, 1H), 10.70 (s, 1H), 7.93 (d, $J = 7.7$ Hz, 2H), 7.61–7.51 (m, 2H), 7.44 (d, $J = 8.1$ Hz, 2H), 7.39 (d, $J = 7.6$ Hz, 1H), 7.31 (t, $J = 7.7$ Hz, 1H), 3.79 (s, 2H), 3.62 (s, 2H), 1.36 (s, 6H). ^{13}C NMR (151 MHz, DMSO- d_6) δ 164.52, 131.32, 130.90, 130.09, 128.79, 128.18, 127.89, 122.14, 59.93, 51.75, 40.54, 24.09. $R_f = 0.20$ (4% Methanol/Dichloromethane). HRMS (ESI, m/z) calcd for $C_{21}H_{21}BrN_4O$ $[M+H]^+$, 425.0977; found 425.0989.

4.1.8.7. *N*-[5-(3-chlorobenzyl)-6,6-dimethyl-1,4,5,6-tetrahydropyrrolo[3,4-*c*]pyrazol-3-yl]benzamide (**17g**). White solid. Yield: 53%. m.p. 193.7–195.0 °C 1H NMR (400 MHz, DMSO- d_6) δ 7.93 (d, $J = 7.6$ Hz, 2H), 7.61–7.44 (m, 2H), 7.43 (s, 1H), 7.40–7.32 (m, 3H), 3.80 (s, 2H), 3.60 (s, 2H), 1.36 (s, 6H). ^{13}C NMR (151 MHz, DMSO- d_6) δ 164.52, 133.46, 130.57, 128.79, 128.43, 128.18, 127.48, 127.18, 59.91, 51.79, 40.53, 24.09. $R_f = 0.21$ (4% Methanol/Dichloromethane). HRMS (ESI, m/z) calcd for $C_{21}H_{21}ClN_4O$ $[M+H]^+$, 381.1482; found 381.1497.

4.1.8.8. *N*-[5-(3-fluorobenzyl)-6,6-dimethyl-1,4,5,6-tetrahydropyrrolo[3,4-*c*]pyrazol-3-yl]benzamide (**17h**). White solid. Yield: 50%. m.p. 143.1–144.1 °C 1H NMR (600 MHz, DMSO- d_6) δ 10.70 (s, 1H), 7.91 (d, $J = 7.7$ Hz, 2H), 7.60–7.44 (m, 3H), 7.42 (d, $J = 1.9$ Hz, 1H), 7.38–7.32 (m, 2H), 7.30 (d, $J = 7.3$ Hz, 1H), 3.79 (s, 2H), 3.59 (s, 2H), 1.35 (s, 6H). ^{13}C NMR (151 MHz, DMSO- d_6) δ 162.22, 160.56 (d, $J = 243.0$ Hz), 141.81, 128.25 (d, $J = 8.2$ Hz), 127.84, 126.49, 125.88, 122.42, 112.88 (d, $J = 21.1$ Hz), 111.64 (d, $J = 20.9$ Hz), 57.58, 49.57, 38.24, 21.82. $R_f = 0.31$ (5% Methanol/Dichloromethane). HRMS (ESI, m/z) calcd for $C_{21}H_{21}FN_4O$ $[M+H]^+$, 365.1778; found 365.1798.

4.1.8.9. *N*-[6,6-dimethyl-5-(3-nitrobenzyl)-1,4,5,6-tetrahydropyrrolo[3,4-*c*]pyrazol-3-yl]benzamide (**17i**). Yellow solid. Yield: 51%. m.p. 178.1–178.8 °C 1H NMR (600 MHz, DMSO- d_6) δ 12.29 (s, 1H), 10.71 (s, 1H), 8.23 (t, $J = 2.1$ Hz, 1H), 8.16–8.09 (m, 1H), 7.91 (d, $J = 7.7$ Hz, 2H), 7.89–7.84 (m, 1H), 7.65 (t, $J = 7.9$ Hz, 1H), 7.59–7.41 (m, 3H),

3.95 (s, 2H), 3.72–3.48 (m, 2H), 1.40 (s, 6H). ^{13}C NMR (151 MHz, DMSO- d_6) δ 164.53, 148.45, 143.55, 135.54, 130.25, 128.79, 128.16, 123.06, 122.32, 60.03, 51.59, 40.53, 24.19. $R_f = 0.88$ (10% Methanol/Dichloromethane). HRMS (ESI, m/z) calcd for $C_{21}H_{21}N_5O_3$ $[M+H]^+$, 392.1723; found 392.1741.

4.1.8.10. *N*-[5-(2-fluorobenzyl)-6,6-dimethyl-1,4,5,6-tetrahydropyrrolo[3,4-*c*]pyrazol-3-yl]benzamide (**17j**). White solid. Yield: 54%. m.p. 193.1–194.2 °C 1H NMR (600 MHz, DMSO- d_6) δ 12.25 (s, 1H), 10.67 (s, 1H), 7.93 (d, $J = 7.5$ Hz, 2H), 7.63–7.37 (m, 4H), 7.31 (tt, $J = 7.3, 3.5$ Hz, 1H), 7.22–7.12 (m, 2H), 3.83 (s, 2H), 3.72–3.49 (m, 2H), 1.36 (s, 6H). ^{13}C NMR (151 MHz, DMSO- d_6) δ 164.54, 161.23 (d, $J = 244.9$ Hz), 131.48 (d, $J = 4.5$ Hz), 129.13 (d, $J = 7.8$ Hz), 128.80, 128.18, 127.22 (d, $J = 13.9$ Hz), 124.70, 124.68, 115.62 (d, $J = 21.7$ Hz), 60.02, 45.26, 40.53, 23.87. $R_f = 0.75$ (10% Methanol/Dichloromethane). HRMS (ESI, m/z) calcd for $C_{21}H_{21}FN_4O$ $[M+H]^+$, 365.1778; found 365.1796.

4.1.8.11. *N*-[5-(4-fluorobenzyl)-6,6-dimethyl-1,4,5,6-tetrahydropyrrolo[3,4-*c*]pyrazol-3-yl]benzamide (**17k**). White solid. Yield: 56%. m.p. 211.5–212.5 °C 1H NMR (600 MHz, DMSO- d_6) δ 12.24 (s, 1H), 10.68 (s, 1H), 7.92 (d, $J = 7.6$ Hz, 2H), 7.61–7.43 (m, 3H), 7.41 (dd, $J = 8.3, 5.6$ Hz, 2H), 7.15 (t, $J = 8.7$ Hz, 2H), 3.77 (s, 2H), 3.70–3.42 (m, 2H), 1.36 (s, 6H). ^{13}C NMR (151 MHz, DMSO- d_6) δ 163.39, 160.51 (d, $J = 241.9$ Hz), 135.77, 129.43 (d, $J = 8.2$ Hz), 127.64, 127.07, 114.25 (d, $J = 21.0$ Hz), 58.72, 50.45, 39.44, 23.00. $R_f = 0.23$ (5% Methanol/Dichloromethane). HRMS (ESI, m/z) calcd for $C_{21}H_{21}FN_4O$ $[M+H]^+$, 365.1778; found 365.1788.

4.1.8.12. *N*-[5-(3,5-difluorobenzyl)-6,6-dimethyl-1,4,5,6-tetrahydropyrrolo[3,4-*c*]pyrazol-3-yl]benzamide (**17l**). Yellow solid. Yield: 58%. m.p. 170.0–171.5 °C 1H NMR (600 MHz, DMSO- d_6) δ 12.28 (s, 1H), 10.73 (s, 1H), 7.93 (d, $J = 7.7$ Hz, 2H), 7.62–7.41 (m, 3H), 7.10 (d, $J = 8.2$ Hz, 3H), 3.82 (s, 2H), 3.65 (s, 2H), 1.36 (s, 6H). ^{13}C NMR (151 MHz, DMSO- d_6) δ 164.54, 162.93 (dd, $J = 245.8, 13.1$ Hz), 146.22 (t, $J = 8.7$ Hz), 132.13, 130.13, 128.79, 128.17, 111.41 (d, $J = 21.5$ Hz), 109.86, 102.57 (t, $J = 25.9$ Hz), 59.95, 51.65, 40.54, 24.17. $R_f = 0.13$ (5% Methanol/Dichloromethane). HRMS (ESI, m/z) calcd for $C_{21}H_{20}F_2N_4O$ $[M+H]^+$, 383.1683; found 383.1707.

4.1.8.13. *N*-[5-(2,3-difluorobenzyl)-6,6-dimethyl-1,4,5,6-tetrahydropyrrolo[3,4-*c*]pyrazol-3-yl]benzamide (**17m**). White solid. Yield: 59%. m.p. 184.1–185.0 °C 1H NMR (600 MHz, DMSO- d_6) δ 12.06 (s, 1H), 10.69 (s, 1H), 7.93 (d, $J = 7.8$ Hz, 2H), 7.46–7.53 (m, 3H), 7.40–7.25 (m, 2H), 7.19 (td, $J = 7.9, 4.7$ Hz, 1H), 3.88 (s, 2H), 3.75–3.49 (m, 1H), 1.36 (s, 6H). ^{13}C NMR (151 MHz, DMSO- d_6) δ 164.55, 150.32 (dd, $J = 205.6, 12.5$ Hz), 148.69 (dd, $J = 206.9, 12.5$ Hz), 130.11 (d, $J = 10.1$ Hz), 134.16, 132.10, 128.79, 128.18, 126.49, 124.97–124.85 (m), 116.20 (d, $J = 16.7$ Hz), 109.83, 60.13, 45.25, 40.53, 23.89. $R_f = 0.25$ (5% Methanol/Dichloromethane). HRMS (ESI, m/z) calcd for $C_{21}H_{20}F_2N_4O$ $[M+H]^+$, 383.1683; found 383.1707.

4.1.8.14. *N*-[5-(2,5-difluorobenzyl)-6,6-dimethyl-1,4,5,6-tetrahydropyrrolo[3,4-*c*]pyrazol-3-yl]benzamide (**17n**). Yellow solid. Yield: 35%. m.p. 111.9–112.6 °C 1H NMR (600 MHz, DMSO- d_6) δ 12.26 (s, 1H), 10.75 (s, 1H), 7.94 (d, $J = 7.7$ Hz, 2H), 7.55 (t, $J = 7.3$ Hz, 1H), 7.47 (t, $J = 7.5$ Hz, 2H), 7.30 (ddd, $J = 9.0, 5.5, 3.2$ Hz, 1H), 7.24 (td, $J = 9.2, 4.4$ Hz, 1H), 7.15 (td, $J = 8.2, 4.1$ Hz, 1H), 3.83 (s, 2H), 3.67 (s, 2H), 1.36 (s, 6H). ^{13}C NMR (151 MHz, DMSO- d_6) δ 155.28, 147.35, 144.37, 138.19, 137.22, 136.47, 132.31, 131.40, 130.26, 130.13, 129.27, 127.50, 60.84, 40.55, 35.16, 19.11. $R_f = 0.29$ (5% Methanol/Dichloromethane). HRMS (ESI, m/z) calcd for $C_{21}H_{20}F_2N_4NaO$ $[M+Na]^+$, 405.1503; found 405.1528.

4.1.8.15. *N*-[5-(3,4-difluorobenzyl)-6,6-dimethyl-1,4,5,6-tetrahydropyrrolo[3,4-*c*]pyrazol-3-yl]benzamide (**17o**). White solid. Yield: 55%. m.p. 177.4–178.5 °C ¹H NMR (600 MHz, DMSO-*d*₆) δ 12.06 (s, 1H), 10.70 (s, 1H), 7.93 (d, *J* = 7.6 Hz, 2H), 7.48–7.51 (m, *J* = 3H), 7.39 (ddt, *J* = 13.7, 11.0, 5.2 Hz, 2H), 7.28–7.18 (m, 1H), 3.78 (s, 2H), 3.62 (s, 2H), 1.36 (s, 6H). ¹³C NMR (151 MHz, DMSO-*d*₆) δ 164.52, 150.14 (dd, *J* = 171.7, 12.6 Hz), 148.52 (dd, *J* = 170.4, 12.7 Hz), 138.80, 134.06, 132.17, 128.80, 128.17, 125.16 (d, *J* = 5.9 Hz), 117.60 (d, *J* = 17.1 Hz), 117.32 (d, *J* = 16.5 Hz), 59.92, 51.29, 40.53, 24.11. *R*_f = 0.26 (5% Methanol/Dichloromethane). HRMS (ESI, *m/z*) calcd for C₂₁H₂₀F₂N₄O [M+H]⁺, 383.1683; found 383.1698.

4.1.8.16. *N*-[5-(2,4-difluorobenzyl)-6,6-dimethyl-1,4,5,6-tetrahydropyrrolo[3,4-*c*]pyrazol-3-yl]benzamide (**17p**). White solid. Yield: 57%. m.p. 186.2–186.9 °C ¹H NMR (600 MHz, DMSO-*d*₆) δ 10.70 (s, 1H), 7.92 (d, *J* = 7.7 Hz, 2H), 7.57–7.41 (m, 4H), 7.18 (td, *J* = 9.9, 2.6 Hz, 1H), 7.06 (td, *J* = 8.4, 2.6 Hz, 1H), 3.79 (s, 2H), 3.61 (s, 2H), 1.34 (s, 6H). ¹³C NMR (151 MHz, DMSO-*d*₆) δ 164.54, 161.82 (dd, *J* = 244.7, 16.1 Hz), 161.06 (dd, *J* = 244.7, 10.9 Hz), 134.06, 132.52 (t, *J* = 7.7 Hz), 132.18, 128.80, 128.18, 123.62, 111.69 (d, *J* = 22.0 Hz), 104.12 (t, *J* = 25.8 Hz), 60.05, 44.89, 40.53, 23.84. *R*_f = 0.26 (5% Methanol/Dichloromethane). HRMS (ESI, *m/z*) calcd for C₂₁H₂₀F₂N₄O [M+H]⁺, 383.1683; found 383.1681.

4.1.8.17. *N*-[5-(2,6-difluorobenzyl)-6,6-dimethyl-1,4,5,6-tetrahydropyrrolo[3,4-*c*]pyrazol-3-yl]benzamide (**17q**). White solid. Yield: 49%. m.p. 215.2–216.1 °C ¹H NMR (600 MHz, DMSO-*d*₆) δ 12.26 (s, 1H), 10.69 (s, 1H), 7.94 (d, *J* = 7.7 Hz, 2H), 7.64–7.44 (m, 3H), 7.39 (ddd, *J* = 14.9, 8.4, 6.5 Hz, 1H), 7.09 (t, *J* = 7.8 Hz, 2H), 3.83 (s, 2H), 3.75–3.55 (m, 2H), 1.37 (s, 6H). ¹³C NMR (151 MHz, DMSO-*d*₆) δ 163.35, 160.58 (dd, *J* = 247.2, 8.3 Hz), 132.88, 130.90, 128.73 (t, *J* = 10.8 Hz), 127.56, 126.96, 114.50 (t, *J* = 18.8 Hz), 110.73 (d, *J* = 4.8 Hz), 110.59 (d, *J* = 4.8 Hz), 58.96, 39.29, 37.78, 22.22. *R*_f = 0.31 (5% Methanol/Dichloromethane). HRMS (ESI, *m/z*) calcd for C₂₁H₂₀F₂N₄O [M+H]⁺, 383.1683; found 383.1676.

4.1.8.18. *N*-[5-(3-fluoro-4-methylbenzyl)-6,6-dimethyl-1,4,5,6-tetrahydropyrrolo[3,4-*c*]pyrazol-3-yl]benzamide (**17r**). White solid. Yield: 51%. m.p. 189.1–190.5 °C ¹H NMR (600 MHz, DMSO-*d*₆) δ 12.23 (s, 1H), 10.69 (s, 1H), 7.91 (d, *J* = 7.7 Hz, 2H), 7.60–7.36 (m, 3H), 7.22 (t, *J* = 7.8 Hz, 1H), 7.12–7.10 (m, 1H), 7.09 (s, 1H), 3.74 (s, 2H), 3.57 (s, 2H), 2.20 (s, 3H), 1.34 (s, 6H). ¹³C NMR (151 MHz, DMSO-*d*₆) δ 163.39, 160.11 (d, *J* = 242.1 Hz), 139.96, 132.97, 131.06, 130.65 (d, *J* = 5.3 Hz), 127.70, 127.07, 123.38, 121.68 (d, *J* = 17.1 Hz), 113.87 (d, *J* = 21.7 Hz), 50.55, 39.44, 22.96, 13.26 (d, *J* = 3.3 Hz). *R*_f = 0.26 (5% Methanol/Dichloromethane). HRMS (ESI, *m/z*) calcd for C₂₂H₂₃FN₄O [M+H]⁺, 379.1934; found 379.1946.

4.1.8.19. *N*-[5-(2-fluoro-5-methylbenzyl)-6,6-dimethyl-1,4,5,6-tetrahydropyrrolo[3,4-*c*]pyrazol-3-yl]benzamide (**17s**). White solid. Yield: 53%. m.p. 184.4–185.3 °C ¹H NMR (600 MHz, DMSO-*d*₆) δ 12.25 (s, 1H), 10.68 (s, 1H), 7.91 (d, *J* = 7.7 Hz, 2H), 7.60–7.38 (m, 3H), 7.17 (dt, *J* = 8.3, 4.6 Hz, 2H), 6.96 (td, *J* = 8.5, 2.9 Hz, 1H), 3.76 (s, 2H), 3.68–3.44 (m, 2H), 2.32 (s, 3H), 1.36 (s, 6H). ¹³C NMR (151 MHz, DMSO-*d*₆) δ 164.55, 161.02 (d, *J* = 240.1 Hz), 140.75 (d, *J* = 6.5 Hz), 134.07, 133.20, 132.16, 131.94 (d, *J* = 7.5 Hz), 128.80, 128.18, 115.97 (d, *J* = 21.4 Hz), 113.50 (d, *J* = 20.8 Hz), 60.08, 50.14, 40.53, 23.79, 18.44. *R*_f = 0.29 (5% Methanol/Dichloromethane). HRMS (ESI, *m/z*) calcd for C₂₂H₂₃FN₄O [M+H]⁺, 379.1934; found 379.1928.

4.1.8.20. *N*-[5-[3,5-bis(trifluoromethyl)benzyl]-6,6-dimethyl-1,4,5,6-tetrahydropyrrolo[3,4-*c*]pyrazol-3-yl]benzamide (**17t**). White solid. Yield: 39%. m.p. 216.0–217.2 °C ¹H NMR (600 MHz, DMSO-*d*₆) δ 11.17 (s, 1H), 10.69 (s, 1H), 8.44 (s, 2H), 8.31 (s, 1H), 7.95–7.91 (m,

2H), 7.72–7.56 (m, 1H), 7.52 (t, *J* = 7.7 Hz, 2H), 4.87 (d, *J* = 10.8 Hz, 1H), 4.75 (dd, *J* = 12.6, 7.2 Hz, 1H), 4.66 (dd, *J* = 12.7, 9.8 Hz, 1H), 4.12 (dd, *J* = 12.7, 5.0 Hz, 1H), 1.89 (s, 3H), 1.66 (s, 3H). *R*_f = 0.35 (5% Methanol/Dichloromethane). HRMS (ESI, *m/z*) calcd for C₂₃H₂₀F₆N₄O [M+H]⁺, 483.1620; found 483.1637.

4.1.8.21. *N*-[5-[3-fluoro-5-(trifluoromethyl)benzyl]-6,6-dimethyl-1,4,5,6-tetrahydropyrrolo[3,4-*c*]pyrazol-3-yl]benzamide (**17u**). White solid. Yield: 55%. m.p. 199.7–201.6 °C ¹H NMR (600 MHz, DMSO-*d*₆) δ 10.72 (s, 1H), 7.92 (d, *J* = 7.6 Hz, 2H), 7.60 (s, 1H), 7.57–7.51 (m, 3H), 7.46 (s, 2H), 3.92 (s, 2H), 3.70–3.52 (m, 2H), 1.37 (s, 6H). ¹³C NMR (151 MHz, DMSO-*d*₆) δ 162.61 (d, *J* = 245.6 Hz), 146.30 (d, *J* = 6.9 Hz), 134.06, 132.17, 131.32 (qd, *J* = 32.6, 8.8 Hz), 128.79, 128.18, 123.95 (dd, *J* = 271.6, 4.0 Hz), 121.21, 119.56 (d, *J* = 21.3 Hz), 111.57 (d, *J* = 24.8 Hz), 60.04, 51.47, 40.53, 24.19. *R*_f = 0.35 (5% Methanol/Dichloromethane). HRMS (ESI, *m/z*) calcd for C₂₁H₂₀F₄N₄O [M+H]⁺, 433.1651; found 433.1674.

4.1.8.22. *N*-[6,6-dimethyl-5-(3,4,5-trifluorobenzyl)-1,4,5,6-tetrahydropyrrolo[3,4-*c*]pyrazol-3-yl]benzamide (**17v**). White solid. Yield: 58%. m.p. 179.1–180.3 °C ¹H NMR (600 MHz, DMSO-*d*₆) δ 12.28 (s, 1H), 10.73 (s, 1H), 7.93 (d, *J* = 7.6 Hz, 2H), 7.67–7.39 (m, 3H), 7.32 (dd, *J* = 8.9, 6.7 Hz, 2H), 3.79 (s, 2H), 3.73–3.43 (m, 2H), 1.35 (s, 6H). ¹³C NMR (151 MHz, DMSO-*d*₆) δ 164.57, 150.70 (ddd, *J* = 246.9, 9.9, 3.7 Hz), 137.87 (dt, *J* = 247.8, 11.3, 9.4 Hz), 134.04, 132.18, 130.13, 128.82, 128.15, 112.67 (d, *J* = 16.8 Hz), 59.97, 51.21, 40.50, 24.16. *R*_f = 0.34 (5% Methanol/Dichloromethane). HRMS (ESI, *m/z*) calcd for C₂₁H₁₉F₃N₄O [M+H]⁺, 401.1589; found 401.1607.

4.1.9. General procedure for the synthesis of target compounds **18a** - **18t**

A solution of various benzoic acid (2.34 mmol) in anhydrous dichloromethane (20 mL) was added oxalyl chloride (0.40 mL, 4.67 mmol) and a catalytic amount of *N,N*-dimethylformamide. The reaction was stirred at room temperature for 6 h. The solvent was removed, and then redissolved in anhydrous tetrahydrofuran (20 mL). The solution was cooled to 0 °C, and *N,N*-diisopropylethylamine (0.58 mL, 3.27 mmol) was added. **14** (0.20 g, 0.47 mmol) was subsequently added dropwise. After addition, the resulting solution was stirred at –20 °C for 2 h. The tetrahydrofuran was removed, and then dissolved in methanol. The solution was stirred at reflux for another 2 h. After the reaction was cooled to room temperature, removal of the solvent gave a residue that was purified by silica chromatography (5%–10% methanol/dichloromethane) to obtain **18a** - **18t** in moderate yield.

4.1.10. General procedure for the synthesis of target compounds **19a** - **19s**

The method of synthesizing compounds **19a** - **19s** were similar to the method of synthesizing compounds **17a** - **17v** except that the starting materials were different.

4.1.10.1. *N*-[5-(2,3-difluorobenzyl)-6,6-dimethyl-1,4,5,6-tetrahydropyrrolo[3,4-*c*]pyrazol-3-yl]-2-naphthamide (**19a**). White solid. Yield: 56%. m.p. 190.0–191.1 °C ¹H NMR (600 MHz, DMSO-*d*₆) δ 12.29 (s, 1H), 10.87 (s, 1H), 8.59 (s, 1H), 8.00 (q, *J* = 12.0, 11.0 Hz, 4H), 7.67–7.56 (m, 2H), 7.37–7.28 (m, 2H), 7.24–7.16 (m, 1H), 3.89 (s, 2H), 3.71 (s, 2H), 1.38 (s, 6H). ¹³C NMR (151 MHz, DMSO-*d*₆) δ 164.56, 150.33 (dd, *J* = 202.7, 12.8 Hz), 148.71 (dd, *J* = 204.0, 12.5 Hz), 134.80, 132.54, 131.33, 130.12, 129.46, 128.82, 128.37, 128.09, 127.27, 126.56, 124.79, 116.24 (d, *J* = 16.9 Hz), 60.17, 45.26, 40.53, 23.87. *R*_f = 0.31 (5% Methanol/Dichloromethane). HRMS (ESI, *m/z*) calcd for C₂₅H₂₂F₂N₄O [M+H]⁺, 433.1840; found 433.1840.

4.1.10.2. *N*-[5-(3,5-difluorobenzyl)-6,6-dimethyl-1,4,5,6-tetrahydropyrrolo[3,4-*c*]pyrazol-3-yl]-2-naphthamide (**19b**).

White solid. Yield: 58%. m.p. 206.9–207.8 °C ¹H NMR (600 MHz, DMSO-*d*₆) δ 12.11 (s, 1H), 10.89 (s, 1H), 8.75–8.51 (m, 1H), 8.11–7.95 (m, 4H), 7.62 (d, *J* = 11.5 Hz, 2H), 7.10 (dd, *J* = 14.4, 8.6 Hz, 3H), 3.84 (s, 2H), 3.78–3.52 (m, 2H), 1.36 (s, 6H). ¹³C NMR (151 MHz, DMSO-*d*₆) δ 163.50, 161.87 (dd, *J* = 245.9, 13.1 Hz), 145.13, 133.74, 131.47, 130.28, 128.39, 127.74, 127.30, 127.03, 126.20, 123.72, 110.41 (d, *J* = 21.1 Hz), 101.54 (t, *J* = 25.8 Hz), 58.93, 50.59, 39.47, 23.08. R_f = 0.32 (5% Methanol/Dichloromethane). HRMS (ESI, *m/z*) calcd for C₂₅H₂₂F₂N₄O [M+H]⁺, 433.1840; found 433.1835.

4.1.10.3. *N*-[5-(3,5-difluorobenzyl)-6,6-dimethyl-1,4,5,6-tetrahydropyrrolo[3,4-*c*]pyrazol-3-yl]quinoline-7-carboxamide (**19c**).

White solid. Yield: 57%. m.p. 245.2–246.1 °C ¹H NMR (600 MHz, DMSO-*d*₆) δ 10.98 (s, 1H), 8.99 (dd, *J* = 4.2, 1.8 Hz, 1H), 8.64 (s, 1H), 8.46 (d, *J* = 8.4 Hz, 1H), 8.23 (dd, *J* = 8.8, 2.0 Hz, 1H), 8.07 (d, *J* = 8.8 Hz, 1H), 7.62 (dd, *J* = 8.4, 4.2 Hz, 1H), 7.16–7.03 (m, 3H), 3.84 (s, 2H), 3.68 (s, 2H), 1.37 (s, 6H). ¹³C NMR (151 MHz, DMSO-*d*₆) δ 162.99, 161.83 (dd, *J* = 241.6, 13.0 Hz), 151.66, 148.17, 145.01, 136.56, 130.77, 128.35, 128.19, 127.30, 126.40, 121.61, 110.39 (dd, *J* = 19.9, 4.0 Hz), 101.51 (t, *J* = 25.8 Hz), 58.95, 50.53, 39.42, 23.04. R_f = 0.12 (5% Methanol/Dichloromethane). HRMS (ESI, *m/z*) calcd for C₂₄H₂₂F₂N₅O [M+H]⁺, 434.1792; found 434.1728.

4.1.10.4. *N*-[5-(2,3-difluorobenzyl)-6,6-dimethyl-1,4,5,6-tetrahydropyrrolo[3,4-*c*]pyrazol-3-yl]-4-fluorobenzamide (**19d**).

White solid. Yield: 47%. m.p. 203.2–204.2 °C ¹H NMR (600 MHz, DMSO-*d*₆) δ 12.28 (s, 1H), 10.74 (s, 1H), 8.01 (d, *J* = 10.0 Hz, 2H), 7.38–7.24 (m, 4H), 7.23–7.13 (m, 1H), 3.88 (s, 2H), 3.73–3.54 (m, 2H), 1.36 (s, 6H). ¹³C NMR (151 MHz, DMSO-*d*₆) δ 163.54 (d, *J* = 249.8 Hz), 162.43, 154.16, 149.24 (dd, *J* = 205.6, 12.5 Hz), 147.62 (dd, *J* = 207.2, 12.7 Hz), 139.31, 129.87 (d, *J* = 9.0 Hz), 129.61, 129.02 (dd, *J* = 10.3, 4.2 Hz), 125.40, 123.83 (t, *J* = 5.6 Hz), 115.13 (d, *J* = 16.9 Hz), 114.64 (d, *J* = 21.8 Hz), 108.74, 59.06, 44.17, 39.45, 22.81. R_f = 0.24 (5% Methanol/Dichloromethane). HRMS (ESI, *m/z*) calcd for C₂₁H₁₉F₃N₄O [M+H]⁺, 401.1589; found 401.1581.

4.1.10.5. *N*-[5-(3,5-difluorobenzyl)-6,6-dimethyl-1,4,5,6-tetrahydropyrrolo[3,4-*c*]pyrazol-3-yl]-4-fluorobenzamide (**19e**).

White solid. Yield: 40%. m.p. 213.7–214.8 °C ¹H NMR (600 MHz, DMSO-*d*₆) δ 12.08 (s, 1H), 10.75 (s, 1H), 8.01 (t, *J* = 6.5 Hz, 2H), 7.48–7.21 (m, 2H), 7.10 (d, *J* = 8.3 Hz, 3H), 3.82 (s, 2H), 3.69–3.55 (m, 2H), 1.36 (s, 6H). R_f = 0.25 (5% Methanol/Dichloromethane). ¹³C NMR (151 MHz, DMSO-*d*₆) δ 165.31 (d, *J* = 305.3 Hz), 162.34, 161.78 (dd, *J* = 246.1, 13.3 Hz), 145.02, 130.99 (d, *J* = 19.4 Hz), 129.78 (d, *J* = 9.0 Hz), 129.43, 128.00, 114.59 (dd, *J* = 21.8, 4.7 Hz), 110.26 (dd, *J* = 21.8, 4.8), 101.43 (t, *J* = 26.0 Hz), 58.85, 50.48, 39.38, 23.00. HRMS (ESI, *m/z*) calcd for C₂₁H₁₉F₃N₄O [M+H]⁺, 401.1589; found 401.1584.

4.1.10.6. 4-Bromo-*N*-[5-(2,3-difluorobenzyl)-6,6-dimethyl-1,4,5,6-tetrahydropyrrolo[3,4-*c*]pyrazol-3-yl]benzamide (**19f**).

White solid. Yield: 52%. m.p. 173.3–174.3 °C ¹H NMR (600 MHz, DMSO-*d*₆) δ 12.29 (s, 1H), 10.80 (s, 1H), 7.87 (d, *J* = 8.3 Hz, 2H), 7.76–7.61 (m, 2H), 7.31 (dt, *J* = 12.1, 7.5 Hz, 2H), 7.19 (td, *J* = 8.0, 4.9 Hz, 1H), 3.87 (s, 2H), 3.76–3.51 (m, 2H), 1.37 (s, 6H). ¹³C NMR (151 MHz, DMSO-*d*₆) δ 162.57, 149.22 (dd, *J* = 205.7, 12.6 Hz), 147.59 (dd, *J* = 206.9, 12.4 Hz), 132.16, 130.73, 129.24, 128.99 (d, *J* = 10.5 Hz), 125.39, 124.88, 123.83 (t, *J* = 6.3, 4.3 Hz), 115.12 (d, *J* = 16.8 Hz), 59.05, 44.14, 39.44, 22.78. R_f = 0.26 (5% Methanol/Dichloromethane). HRMS (ESI, *m/z*) calcd for C₂₁H₁₉BrF₂N₄O [M+H]⁺, 461.0789; found 461.0771.

4.1.10.7. 4-Bromo-*N*-[5-(3,5-difluorobenzyl)-6,6-dimethyl-1,4,5,6-tetrahydropyrrolo[3,4-*c*]pyrazol-3-yl]benzamide (**19g**).

White solid.

Yield: 54%. m.p. 204.0–204.8 °C ¹H NMR (400 MHz, DMSO-*d*₆) δ 12.11 (s, 1H), 10.84 (s, 1H), 7.87 (d, *J* = 8.1 Hz, 2H), 7.67 (d, *J* = 7.0 Hz, 2H), 7.10 (dd, *J* = 7.0, 3.7 Hz, 3H), 3.82 (s, 2H), 3.64 (s, 2H), 1.35 (s, 6H). ¹³C NMR (151 MHz, DMSO-*d*₆) δ 162.69, 161.81 (dd, *J* = 236.0, 14.3 Hz), 145.10, 132.18, 130.72, 129.23, 124.86, 110.31 (d, *J* = 21.7 Hz), 101.49 (t, *J* = 25.8 Hz), 58.88, 50.53, 39.44, 23.06. R_f = 0.42 (5% Methanol/Dichloromethane). HRMS (ESI, *m/z*) calcd for C₂₁H₁₉BrF₂N₄O [M+H]⁺, 461.0789; found 461.0772.

4.1.10.8. *N*-[5-(2,3-difluorobenzyl)-6,6-dimethyl-1,4,5,6-tetrahydropyrrolo[3,4-*c*]pyrazol-3-yl]-4-morpholinobenzamide (**19h**).

White solid. Yield: 53%. m.p. 117.4–118.3 °C ¹H NMR (600 MHz, DMSO-*d*₆) δ 12.19 (s, 1H), 10.40 (s, 1H), 7.84 (d, *J* = 8.1 Hz, 2H), 7.35–7.28 (m, 2H), 7.22–7.16 (m, 1H), 6.96 (s, 2H), 3.87 (s, 2H), 3.77–3.70 (m, 4H), 3.63 (s, 2H), 3.23 (t, *J* = 5.0 Hz, 4H), 1.35 (s, 6H). ¹³C NMR (151 MHz, DMSO-*d*₆) δ 163.00, 152.59, 149.21 (dd, *J* = 205.3, 12.8 Hz), 147.59 (dd, *J* = 206.7, 12.7 Hz), 129.04 (d, *J* = 10.1 Hz), 128.47, 125.39, 123.81 (t, *J* = 5.5 Hz), 115.08 (d, *J* = 17.0 Hz), 112.62, 65.28, 58.98, 46.54, 44.16, 39.43, 22.77. R_f = 0.75 (10% Methanol/Dichloromethane). HRMS (ESI, *m/z*) calcd for C₂₅H₂₇F₂N₅O₂ [M+H]⁺, 468.2211; found 468.2214.

4.1.10.9. *N*-[5-(3,5-difluorobenzyl)-6,6-dimethyl-1,4,5,6-tetrahydropyrrolo[3,4-*c*]pyrazol-3-yl]-4-morpholinobenzamide (**19i**).

White solid. Yield: 53%. m.p. 125.3–126.1 °C ¹H NMR (600 MHz, DMSO-*d*₆) δ 12.20 (s, 1H), 10.64–10.27 (m, 1H), 7.84 (d, *J* = 8.4 Hz, 2H), 7.13–7.05 (m, 3H), 6.96 (s, 2H), 3.82 (s, 2H), 3.76–3.69 (m, 4H), 3.61 (s, 3H), 3.23 (t, *J* = 4.9 Hz, 4H), 1.34 (s, 6H). ¹³C NMR (151 MHz, DMSO-*d*₆) δ 164.08, 162.93 (dd, *J* = 245.6, 13.2 Hz), 153.69, 146.26 (t, *J* = 8.5 Hz), 129.56, 123.30, 113.72, 111.41 (dd, *J* = 20.1, 4.5 Hz), 102.55 (t, *J* = 26.0 Hz), 66.38, 59.90, 51.68, 47.63, 40.53, 24.15. R_f = 0.75 (10% Methanol/Dichloromethane). HRMS (ESI, *m/z*) calcd for C₂₅H₂₇F₂N₅O₂ [M+H]⁺, 468.2211; found 468.2213.

4.1.10.10. *N*-[5-(2,3-difluorobenzyl)-1,4,5,6-tetrahydropyrrolo[3,4-*c*]pyrazol-3-yl]-4-(dimethylamino)benzamide (**19j**).

Yellow solid. Yield: 51%. m.p. 110.0–111.3 °C ¹H NMR (600 MHz, DMSO-*d*₆) δ 12.15 (s, 1H), 10.29 (s, 1H), 7.82 (d, *J* = 8.6 Hz, 2H), 7.37–7.28 (m, 2H), 7.22–7.17 (m, 1H), 6.75–6.64 (m, 2H), 3.87 (s, 2H), 3.61 (s, 2H), 2.97 (s, 6H), 1.35 (s, 6H). ¹³C NMR (151 MHz, DMSO-*d*₆) δ 163.23, 151.82, 149.22 (dd, *J* = 205.5, 12.9 Hz), 147.60 (dd, *J* = 206.7, 12.6 Hz), 129.07 (d, *J* = 10.1 Hz), 128.55, 125.41, 123.82 (t, *J* = 5.7 Hz), 119.16, 115.09 (d, *J* = 16.9 Hz), 110.11, 58.97, 44.18, 39.44, 22.78. R_f = 0.66 (10% Methanol/Dichloromethane). HRMS (ESI, *m/z*) calcd for C₂₃H₂₅F₂N₅O [M+H]⁺, 426.2105; found 426.2109.

4.1.10.11. *N*-[5-(3,5-difluorobenzyl)-1,4,5,6-tetrahydropyrrolo[3,4-*c*]pyrazol-3-yl]-4-(dimethylamino)benzamide (**19k**).

Yellow solid. Yield: 55%. m.p. 179.1–180.3 °C ¹H NMR (600 MHz, DMSO-*d*₆) δ 10.30 (s, 1H), 7.82 (d, *J* = 8.4 Hz, 2H), 7.13–7.06 (m, 3H), 6.69 (d, *J* = 8.1 Hz, 2H), 3.81 (s, 2H), 3.60 (s, 2H), 2.97 (s, 6H), 1.34 (s, 6H). ¹³C NMR (151 MHz, DMSO-*d*₆) δ 163.22, 161.84 (dd, *J* = 245.8, 13.0 Hz), 151.82, 145.19 (t, *J* = 8.4 Hz), 128.54, 119.20, 110.32 (dd, *J* = 20.6, 4.5 Hz), 110.11, 101.46 (t, *J* = 26.0 Hz), 58.80, 50.60, 39.44, 23.06. R_f = 0.66 (10% Methanol/Dichloromethane). HRMS (ESI, *m/z*) calcd for C₂₃H₂₅F₂N₅O [M+H]⁺, 426.2105; found 426.2098.

4.1.10.12. *N*-[5-(2,3-difluorobenzyl)-6,6-dimethyl-1,4,5,6-tetrahydropyrrolo[3,4-*c*]pyrazol-3-yl]-4-(4-methylpiperazin-1-yl)benzamide (**19l**).

White solid. Yield: 49%. m.p. 192.1–193.5 °C ¹H NMR (600 MHz, DMSO-*d*₆) δ 12.16 (s, 1H), 10.38 (s, 1H), 7.82 (d, *J* = 7.4 Hz, 2H), 7.31 (td, *J* = 10.5, 9.3, 4.3 Hz, 2H), 7.23–7.17 (m, 1H), 6.94 (s, 1H), 3.87 (s, 2H), 3.62 (s, 2H), 3.26 (s, 4H), 2.47–2.40 (m, 4H), 2.21 (s, 3H), 1.35 (s, 6H). ¹³C NMR (151 MHz, DMSO-*d*₆) δ 164.09, 153.54, 150.31 (dd, *J* = 205.8, 12.4 Hz), 148.68 (dd, *J* = 206.9,

12.5 Hz), 130.15 (d, $J = 9.7$ Hz), 129.58, 126.50, 124.91 (t, $J = 5.7$ Hz), 116.18 (d, $J = 16.9$ Hz), 113.84, 60.07, 54.83, 47.28, 46.19, 45.26, 40.54, 23.87. $R_f = 0.24$ (10% Methanol/Dichloromethane). HRMS (ESI, m/z) calcd for $C_{26}H_{30}F_2N_6O$ $[M+H]^+$, 481.2527; found 481.2531.

4.1.10.13. *N*-[5-(3,5-difluorobenzyl)-6,6-dimethyl-1,4,5,6-tetrahydropyrrolo[3,4-*c*]pyrazol-3-yl]-4-(4-methylpiperazin-1-yl) benzamide (**19m**). White solid. Yield: 58%. m.p. 200.9–202.0 °C 1H NMR (600 MHz, DMSO- d_6) δ 12.18 (s, 1H), 10.39 (s, 1H), 7.82 (d, $J = 8.4$ Hz, 2H), 7.13–7.06 (m, 3H), 6.99–6.85 (m, 2H), 3.81 (s, 2H), 3.59 (s, 2H), 3.26 (t, $J = 5.1$ Hz, 4H), 2.43 (t, $J = 5.0$ Hz, 4H), 2.21 (s, 3H), 1.34 (s, 6H). ^{13}C NMR (151 MHz, DMSO- d_6) δ 164.09, 162.93 (dd, $J = 245.7, 13.2$ Hz), 153.48, 146.28 (d, $J = 8.8$ Hz), 130.13, 129.65, 129.58, 122.80, 114.10, 113.88, 111.41 (dd, $J = 19.9, 4.6$ Hz), 102.56 (t, $J = 25.9$ Hz), 59.91, 54.71, 51.67, 47.16, 46.02, 40.51, 24.14. $R_f = 0.23$ (10% Methanol/Dichloromethane). HRMS (ESI, m/z) calcd for $C_{26}H_{30}F_2N_6O$ $[M+H]^+$, 481.2527; found 481.2526.

4.1.10.14. 1-(3,5-difluorobenzyl)-4-(4-[[5-(3,5-difluorobenzyl)-6,6-dimethyl-1,4,5,6-tetrahydropyrrolo[3,4-*c*]pyrazol-3-yl]carbonyl]phenyl)-1-methylpiperazin-1-ium (**19n**). White solid. Yield: 37%. Decompose without heating to the m.p. 1H NMR (600 MHz, DMSO- d_6) δ 10.51 (s, 1H), 7.91 (d, $J = 8.5$ Hz, 2H), 7.52 (tt, $J = 9.3, 2.4$ Hz, 1H), 7.41–7.36 (m, 2H), 7.13–7.03 (m, 5H), 4.72 (s, 2H), 3.96–3.87 (m, 2H), 3.82 (s, 2H), 3.62 (dd, $J = 13.3, 9.9$ Hz, 4H), 3.51 (td, $J = 12.8, 10.9, 3.2$ Hz, 4H), 3.11 (s, 3H), 1.35 (s, 6H). ^{13}C NMR (151 MHz, DMSO- d_6) δ 163.89, 162.93 (dd, $J = 245.8, 13.1$ Hz), 162.76 (dd, $J = 247.5, 13.4$ Hz), 158.30 (d, $J = 30.4$ Hz), 152.03, 146.27, 131.47 (t, $J = 10.0$ Hz), 130.13, 129.66, 118.85, 117.26–116.91 (m), 116.86 (dd, $J = 18.9, 5.4$ Hz), 114.45, 111.41 (d, $J = 23.3$ Hz), 106.66 (t, $J = 25.6$ Hz), 102.56 (t, $J = 25.9$ Hz), 66.09, 59.92, 59.05, 51.67, 45.34, 41.33, 40.53, 24.15. $R_f = 0.66$ (50% Methanol/Dichloromethane). HRMS (ESI, m/z) calcd for $C_{33}H_{37}F_2N_6O$ $[M+H]^+$, 608.2887; found 608.2848.

4.1.10.15. *N*-[5-(2,3-difluorobenzyl)-6,6-dimethyl-1,4,5,6-tetrahydropyrrolo[3,4-*c*]pyrazol-3-yl]-3-morpholinobenzamide (**19o**). White solid. Yield: 44%. m.p. 182.1–183.6 °C 1H NMR (600 MHz, DMSO- d_6) δ 12.25 (s, 1H), 10.66 (s, 1H), 7.48 (s, 1H), 7.39–7.27 (m, 4H), 7.23–7.16 (m, 1H), 7.11 (d, $J = 8.1$ Hz, 1H), 3.88 (s, 2H), 3.79–3.63 (m, 4H), 3.65 (s, 2H), 3.16 (dd, $J = 5.8, 3.9$ Hz, 4H), 1.37 (s, 6H). ^{13}C NMR (151 MHz, DMSO- d_6) δ 164.69, 151.46, 150.32 (dd, $J = 205.6, 12.6$ Hz), 148.69 (dd, $J = 207.1, 12.8$ Hz), 134.73, 130.12 (d, $J = 10.0$ Hz), 129.44, 126.48, 124.93 (t, $J = 5.9$ Hz), 118.91, 118.67, 116.20 (d, $J = 16.6$ Hz), 114.48, 66.51, 60.11, 48.76, 45.24, 40.54, 23.89. $R_f = 0.79$ (10% Methanol/Dichloromethane). HRMS (ESI, m/z) calcd for $C_{25}H_{27}F_2N_5O_2$ $[M+H]^+$, 468.2211; found 468.2208.

4.1.10.16. *N*-[5-(3,5-difluorobenzyl)-6,6-dimethyl-1,4,5,6-tetrahydropyrrolo[3,4-*c*]pyrazol-3-yl]-3-morpholinobenzamide (**19p**). White solid. Yield: 41%. m.p. 192.5–193.6 °C 1H NMR (600 MHz, DMSO- d_6) δ 12.27 (s, 1H), 10.67 (s, 1H), 7.50 (s, 1H), 7.36 (s, 1H), 7.30 (s, 1H), 7.14–7.06 (m, 4H), 3.82 (s, 2H), 3.79–3.69 (m, 4H), 3.64 (s, 2H), 3.24–3.10 (m, 4H), 1.35 (s, 6H). ^{13}C NMR (151 MHz, DMSO- d_6) δ 164.67, 162.94 (dd, $J = 245.3, 13.0$ Hz), 155.12, 151.46, 146.24 (t, $J = 8.4$ Hz), 140.61, 134.75, 129.42, 118.94, 114.49, 111.40 (dd, $J = 20.2, 4.6$ Hz), 102.58 (t, $J = 26.1$ Hz), 66.51, 59.94, 51.66, 48.76, 40.54, 24.18. $R_f = 0.67$ (10% Methanol/Dichloromethane). HRMS (ESI, m/z) calcd for $C_{25}H_{27}F_2N_5O_2$ $[M+H]^+$, 468.2211; found 468.2214.

4.1.10.17. *N*-[5-(2,3-difluorobenzyl)-6,6-dimethyl-1,4,5,6-tetrahydropyrrolo[3,4-*c*]pyrazol-3-yl]-3-(dimethylamino)benzamide (**19q**). White solid. Yield: 47%. m.p. 99.3–101.2 °C 1H NMR (600 MHz, DMSO- d_6) δ 12.24 (s, 1H), 10.60 (s, 1H), 7.36–7.15 (m, 6H),

6.94–6.84 (m, 1H), 3.88 (s, 2H), 3.65 (s, 2H), 2.93 (s, 6H), 1.36 (s, 6H). ^{13}C NMR (151 MHz, DMSO- d_6) δ 164.00, 149.64, 149.21 (dd, $J = 206.2, 12.7$ Hz), 147.58 (dd, $J = 207.4, 12.7$ Hz), 133.59, 129.03 (d, $J = 9.9$ Hz), 128.20, 125.36, 123.82 (t, $J = 5.9, 5.3$ Hz), 115.08 (d, $J = 16.5$ Hz), 114.72, 110.66, 58.99, 44.14, 39.48, 39.43, 22.78. $R_f = 0.67$ (10% Methanol/Dichloromethane). HRMS (ESI, m/z) calcd for $C_{23}H_{25}F_2N_5O$ $[M+H]^+$, 426.2105; found 426.2108.

4.1.10.18. *N*-[5-(3,5-difluorobenzyl)-6,6-dimethyl-1,4,5,6-tetrahydropyrrolo[3,4-*c*]pyrazol-3-yl]-3-(dimethylamino)benzamide (**19r**). White solid. Yield: 45%. m.p. 110.3–111.5 °C 1H NMR (600 MHz, DMSO- d_6) δ 10.60 (s, 1H), 7.28–7.14 (m, 3H), 7.13–7.04 (m, 3H), 6.88 (d, $J = 7.9$ Hz, 1H), 3.82 (s, 2H), 3.62 (s, 2H), 2.93 (s, 6H), 1.35 (s, 6H). ^{13}C NMR (151 MHz, DMSO- d_6) δ 165.09, 162.94 (dd, $J = 245.7, 13.1$ Hz), 150.75, 146.26 (t, $J = 8.5$ Hz), 134.68, 130.14, 115.81 (d, $J = 12.7$ Hz), 111.77, 111.40 (dd, $J = 17.7, 4.7$ Hz), 102.58 (t, $J = 25.9$ Hz), 59.93, 51.66, 40.59, 40.54, 24.17. $R_f = 0.68$ (10% Methanol/Dichloromethane). HRMS (ESI, m/z) calcd for $C_{23}H_{25}F_2N_5O$ $[M+H]^+$, 426.2105; found 426.2115.

4.1.10.19. *N*-[5-(2,3-difluorobenzyl)-6,6-dimethyl-1,4,5,6-tetrahydropyrrolo[3,4-*c*]pyrazol-3-yl]-3-(4-methylpiperazin-1-yl) benzamide (**19s**). White solid. Yield: 48%. m.p. 113.6–114.5 °C 1H NMR (600 MHz, DMSO- d_6) δ 12.23 (s, 1H), 10.64 (s, 1H), 7.47 (s, 1H), 7.35–7.26 (m, 4H), 7.22–7.17 (m, 1H), 7.10 (d, $J = 8.1$ Hz, 1H), 3.88 (s, 2H), 3.64 (s, 2H), 3.19 (d, $J = 5.2$ Hz, 4H), 2.47 (d, $J = 5.2$ Hz, 4H), 2.23 (s, 3H), 1.36 (s, 6H). $R_f = 0.11$ (10% Methanol/Dichloromethane). HRMS (ESI, m/z) calcd for $C_{26}H_{30}F_2N_6O$ $[M+H]^+$, 481.2527; found 481.2527.

4.1.10.20. *N*-[5-(3,5-difluorobenzyl)-6,6-dimethyl-1,4,5,6-tetrahydropyrrolo[3,4-*c*]pyrazol-3-yl]-3-(4-methylpiperazin-1-yl) benzamide (**19t**). White solid. Yield: 55%. m.p. 114.7–115.4 °C 1H NMR (600 MHz, DMSO- d_6) δ 12.26 (s, 1H), 10.66 (s, 1H), 7.48 (s, 1H), 7.33 (d, $J = 6.8$ Hz, 1H), 7.28 (s, 1H), 7.10 (d, $J = 7.9$ Hz, 4H), 3.82 (s, 2H), 3.63 (s, 2H), 3.25–3.11 (m, 4H), 2.46 (s, 4H), 2.23 (s, 3H), 1.35 (s, 6H). ^{13}C NMR (151 MHz, DMSO- d_6) δ 164.71, 162.93 (dd, $J = 245.4, 13.4$ Hz), 151.32, 146.25, 134.71, 130.13, 129.39, 118.82, 118.55, 114.72, 111.78–110.98 (m), 102.58 (dd, $J = 20.8, 4.1$ Hz), 59.94, 54.93, 51.66, 48.28, 46.12 (d, $J = 6.2$ Hz), 40.54, 24.18. $R_f = 0.11$ (10% Methanol/Dichloromethane). HRMS (ESI, m/z) calcd for $C_{26}H_{30}F_2N_6O$ $[M+H]^+$, 481.2527; found 481.2522.

4.2. Pharmacological assay

4.2.1. TRKs HTRF assay

The purified kinases were purchased from Carna Biosciences (Japan) and the TK kinEASE kit was commercially purchased from Cisbio Bioassays (France). The HTRF assays were performed according to the instructions of manufactures. A few optimization experiments were implemented to find the optimal concentration of kinases. The concentrations of TRKA, TRKB and TRKC used were 0.111 ng/uL, 0.037 ng/uL and 0.037 ng/uL, respectively. The concentrations of ATP were determined by similar experiments, and the concentrations of ATP were 14.68 μ M (TRKA), 4.77 μ M (TRKB) and 25.64 μ M (TRKC).

First, compounds were diluted from a concentrated stock of 8 mM in 100% DMSO and with serial kinase reaction buffer dilutions. Second, a 5 μ M TK solution, 0.5 μ M XL-665 solution, kinases solutions and ATP solutions whose concentrations were displayed in the previous were prepared. For each assays, 4 μ L of dispensed compounds, 2 μ L of ATP, 2 μ L of substrate TK and 2 μ L of kinase were added to the assay wells. The assay wells were incubated at 25 °C for 30–40 min. The enzymatic reaction time was related to the type of kinase. (The reaction time of TRKA was 30 min, however the

reaction time of TRKB and TRKC were 40 min) Finally, a mixture of 5 μ L of XL-665 and 5 μ L of TK-Antibody-Cryptate was added to terminate reactions. The assay well were incubated at 25 °C for another 60 min, and then HTRF signals were obtained by reading plates using as Infinite® F500 microplate reader (Tecan, Switzerland). The ratio of fluorescence at 665 nm to fluorescence at 620 nm was calculated for each well. The data were analysed using Graphpad prism 8. Every experiment was repeated at least two times.

4.2.2. Cell proliferation assay

The antiproliferative activities of the compounds were evaluated against Km-12, A549 and THLE-2 cell lines by the standard Cell Counts Kit-8 (CCK-8) assay *in vitro*. Cells were seeded in 96 well plates. After incubation 24 h, the cells were exposed to various concentrations of compounds for addition 72 h. The IC₅₀ values were calculated by concentration-response curve fitting using prism 8.

4.2.3. Flow cytometry

The FITC-Annexin V and PI apoptosis kit was purchased from US Everbright® Inc. (item: F6012), and the experimental operation was carried out according to the protocol provided by the manufacturer. Briefly, Km-12 cells were incubated with compound **19m** (0.0625, 0.125, 0.25, 0.5, or 1 μ M) for 48 h; then, the cells were digested by trypsin, harvested, and washed twice with PBS. The cells were counted, and 105 cells were dispersed in 100 μ L of Annexin V binding buffer solution, followed by the addition of 4 μ L of FITC-Annexin V working fluid and 2 μ L of PI working fluid to the solution. After incubation at room temperature in the dark for 10 min, 400 μ L of PBS were added, and the fluorescence intensity was detected by flow cytometry (FITC-Annexin V: Abs/Em = 494/518 nm, PI: Abs/Em = 535/617 nm).

4.2.4. Plasma stability assay

The pooled frozen human plasma (BioreclamationIVT, batch No. BRH1569252) was thawed in a water bath at 37 °C prior to experiment. Plasma was centrifuged at 4000 rpm for 5 min and the clots were removed if any. The pH will be adjusted to 7.4 ± 0.1 if required. 100 μ M propantheline bromide solution was prepared by diluting 5 μ L of 10 mM stock solution with 495 μ L H₂O as a positive control. The other detected compound solution was prepared by the same method. 98 μ L of blank plasma was spiked with 2 μ L of dosing solution (100 μ M) to achieve 2 μ M of the final concentration in duplicate and samples were incubated at 37 °C in a water bath. At each time point (0, 10, 30, 60 and 120min), 400 μ L of stop solution (200 ng/mL tolbutamide and 200 ng/mL Labetalol in ACN) was added to precipitate protein and mixed thoroughly. Centrifuged sample plates at 4000 rpm for 15 min. An aliquot of supernatant (50 μ L) was transferred from each well and mixed with 100 μ L ultra pure water. The samples were shaken at 800 rpm for about 10 min before submitting to LC-MS/MS analysis.

4.2.5. Liver microsomal stability assay

The empty 'Incubation' plates T60 and NCF60 were pre-warmed for 10 min. The liver microsomes (Human, Corning, Lot No.38295) was diluted to 0.59 mg/mL as working solutions in 100 mM potassium phosphate buffer. 445 μ L of working solutions were transferred into pre-warmed 'Incubation' plates T60 and NCF60. Then, both of plates were shook at 37 °C for 10 min, 5 μ L of compound working solution (100 μ M) was added and mixed three times thoroughly after 54 μ L of liver microsomes was transferred to another black plate. To the black plate, 6 μ L of NADPH solution (NADPH powder which purchased from Chem-Impex International, Cat No.00616 diluted into 10 mM MgCl₂ solution) and 180 μ L

quenching solution which containing 200 ng/mL tolbutamide and 200 ng/mL labetalol in acetonitrile were added sequentially. 50 μ L of buffer was added to the NCF60 plate, mixed three times thoroughly, and then the plate will be incubated at 37 °C for 60 min while shaking. 44 μ L of NADPH cofactor was added to the T60 plate, and then the plate will be incubated at 37 °C for 60 min as well. At 5, 15, 30, 45, and 60 min, add 180 μ L quenching solution to 'Quenching' plates, mix once, and serially transfer 60 μ L sample from T60 plate per time point to 'Quenching' plates. All sampling plates are shaken for 10 min, then centrifuged at 4000 rpm for 20 min at 4 °C, and 80 μ L of supernatant was removed into 240 μ L pure water and mixed by plate shaker for 10 min. Each bioanalysis plate was sealed and shaken for 10 min prior to LC-MS/MS analysis.

4.2.6. Cytochrome P450 inhibition assay

Cytochrome P450 inhibition was evaluated in human liver microsomes (0.253 mg/mL) using five probe substrates (CYP1A2, phenacetin; CYP2C9, diclofenac; CYP2C19, S-mephenytoin; CYP2D6, dextromethorphan; and CYP3A4, midazolam.) in the presence of compound **19m** (10 μ M). After preincubation for 10 min at 37 °C, an NADPH-regenerating system was added. After the mixed system was incubated for 15 min at 37 °C, the reaction was stopped by adding 400 μ L of cold stop solution (200 ng/mL tolbutamide and 200 ng/mL labetalol in acetonitrile). The incubation mixtures were then centrifuged, and supernatants were analyzed by LC-MS/MS.

4.2.7. Pharmacokinetic study in SD rats

Pharmacokinetic properties were investigated in SD rats (n = 3, pear group) after single intravenous (1 mg/kg) and oral administration (3 mg/kg). The blood samples were collected in heparin-containing tubes at specified time points and centrifuged immediately at 4 °C and 4000 rpm for 20 min. Noncompartmental pharmacokinetic parameters were fitted using phoenix WinNonlin 6.3 based on the LC-MS/MS quantitation data.

4.2.8. Molecular docking study

The TRKA crystal structure (PDB code: 5KVT), which was downloaded from protein data bank (<https://www.rcsb.org/>), was processed with the Protein Preparation Wizard in the Schrödinger suite. The protein structure was adjusted and modified, followed by adding hydrogen atoms, deleting solvent water molecules, and defining right bonds orders using Prime. The protonation and tautomeric states of Asp, Lys, and His were assigned at pH 7.4 state. Afterward, all hydrogen atoms of TRKA complexes were optimized with OPLS_2005 force field, which minimized and converged heavy atoms to a RMSD of 0.3. The selected inhibitors were prepared by using LigPrep from the Schrödinger suite with the OPLS_2005 force field. The structure of inhibitors was also adjusted and modified, followed by adding all hydrogen atoms, checking the bond order and atom types.

Receptor grids were generated before docking with allosteric site determined by the literatures. The prepared protein–ligand complex was imported into Glide 9.7, which defined it as the receptor structure with size box (15 Å × 15 Å × 15 Å). Based on the OPLS_2005 force field, the grid of TRKA crystal structure was generated. The extra precision (XP) mode was set for docking studies with two crucial residues Glu-590 and Met-592 in constrained binding to get accurate results.

Declaration of competing interest

The authors declare that they have no known competing financial interests or personal relationships that could have appeared to influence the work reported in this paper.

Acknowledgment

We gratefully acknowledge the Program for Innovative Research Team of the Ministry of Education and the Program for Liaoning Innovative Research Team in University.

Appendix A. Supplementary data

Supplementary data to this article can be found online at <https://doi.org/10.1016/j.ejmech.2021.113627>.

References

- [1] K. Bartkowska, A. Paquin, A.S. Gauthier, D.R. Kaplan, F.D. Miller, Trk signaling regulates neural precursor cell proliferation and differentiation during cortical development, *Development* 134 (2007) 4369–4380.
- [2] O. Islam, T.X. Loo, K. Heese, Brain-derived neurotrophic factor (BDNF) has proliferative effects on neural stem cells through the truncated TRK-B receptor, MAP kinase, AKT, and STAT-3 signaling pathways, *Curr. Neurovascular Res.* 6 (2009) 42–53.
- [3] F. Barnabe-Heider, F.D. Miller, Endogenously produced neurotrophins regulate survival and differentiation of cortical progenitors via distinct signaling pathways, *J. Neurosci.* 23 (2003) 5149–5160.
- [4] M.V. Chao, Neurotrophins and their receptors: a convergence point for many signalling pathways, *Nat. Rev. Neurosci.* 4 (2003) 299–309.
- [5] A.A. Bapat, G. Hostetter, D.D. Von Hoff, H. Han, Perineural invasion and associated pain in pancreatic cancer, *Nat. Rev. Canc.* 11 (2011) 695–707.
- [6] E.J. Huang, L.F. Reichardt, Neurotrophins: roles in neuronal development and function, *Annu. Rev. Neurosci.* 24 (2001) 677–736.
- [7] M.H. Ultsch, C. Wiesmann, L.C. Simmons, J. Henrich, M. Yang, D. Reilly, S.H. Bass, A.M. de Vos, Crystal structures of the neurotrophin-binding domain of TrkA, TrkB and TrkC, *J. Mol. Biol.* 290 (1999) 149–159.
- [8] C. Wiesmann, M.H. Ultsch, S.H. Bass, A.M. de Vos, Crystal structure of nerve growth factor in complex with the ligand-binding domain of the TrkA receptor, *Nature* 401 (1999) 184–188.
- [9] T. Bertrand, M. Kothe, J. Liu, A. Dupuy, A. Rak, P.F. Berne, S. Davis, T. Gladysheva, C. Valtre, J.Y. Crenne, M. Mathieu, The crystal structures of trkA and trkB suggest key regions for achieving selective inhibition, *J. Mol. Biol.* 423 (2012) 439–453.
- [10] D.R. Kaplan, B.L. Hempstead, D. Martin-Zanca, M.V. Chao, L.F. Parada, The trk proto-oncogene product: a signal transducing receptor for nerve growth factor, *Science* 252 (1991) 554–558.
- [11] D.R. Kaplan, D. Martin-Zanca, L.F. Parada, Tyrosine phosphorylation and tyrosine kinase activity of the TRK proto-oncogene product induced by NGF, *Nature* 350 (1991) 158–160.
- [12] R. Klein, V. Nanduri, S.A. Jing, F. Lamballe, P. Tapley, S. Bryant, et al., The TRKB tyrosine protein kinase is a receptor for brain-derived neurotrophic factor and neurotrophin-3, *Cell* 66 (1991) 395–403.
- [13] A. Amatu, A. Sartore-Bianchi, S. Siena, NTRK gene fusions as novel targets of cancer therapy across multiple tumour types, *ESMO Open* 1 (2016) e000023.
- [14] A. Greco, C. Miranda, M.A. Pierotti, Rearrangements of NTRK1 gene in papillary thyroid carcinoma, *Mol. Cell. Endocrinol.* 321 (2010) 44–49.
- [15] V. Ranzi, S.O. Meakin, C. Miranda, P. Mondellini, M.A. Pierotti, A. Greco, The signaling adapters fibroblast growth factor receptor substrate 2 and 3 are activated by the thyroid TRK oncoproteins, *Endocrinology* 144 (2003) 922–928.
- [16] C. Miranda, A. Greco, C. Miele, M.A. Pierotti, E. Van Obberghen, IRS-1 and IRS-2 are recruited by TrkA receptor and oncogenic TRK-T1, *J. Cell. Physiol.* 186 (2001) 35–46.
- [17] E. Roccato, C. Miranda, V. Ranzi, M. Gishizki, M.A. Pierotti, A. Greco, Biological activity of the thyroid TRK-T3 oncogene requires signalling through Shc, *Br. J. Canc.* 87 (2002) 645–653.
- [18] T. Wang, M.L. Lamb, D.A. Scott, H. Wang, M.H. Block, P.D. Lyne, J.W. Lee, A.M. Davies, H.J. Zhang, Y. Zhu, F. Gu, Y. Han, B. Wang, P.J. Mohr, R.J. Kaus, J.A. Josey, E. Hoffmann, K. Thress, T. Macintyre, H. Wang, C.A. Omer, D. Yu, Identification of 4-aminopyrazolopyrimidines as potent inhibitors of Trk kinases, *J. Med. Chem.* 51 (2008) 4672–4684.
- [19] T. Wang, M.L. Lamb, M.H. Block, A.M. Davies, Y.X. Han, E. Hoffmann, S. Ioannidis, J.A. Josey, Z.Y. Liu, P.D. Lyne, T. Macintyre, P.J. Mohr, C.A. Omer, K. Thress, B. Wang, H.Y. Wang, D.W. Yu, H.J. Zhang, Discovery of disubstituted imidazo 4,5-b pyridines and purines as potent TrkA inhibitors, *ACS Med. Chem. Lett.* 3 (2012) 705–709.
- [20] M. Menichincheri, E. Ardini, P. Magnaghi, N. Avanzi, P. Banfi, R. Bossi, L. Buffa, G. Canevari, L. Ceriani, M. Colombo, L. Corti, D. Donati, M. Fasolini, E. Felder, C. Fiorelli, F. Fiorentini, A. Galvani, A. Isacchi, A.L. Borgia, C. Marchionni, M. Nesi, C. Orrenius, A. Panzeri, E. Pesenti, L. Rusconi, M.B. Saccardo, E. Vanotti, E. Perrone, P. Orsini, Discovery of entrectinib: a new 3- aminoindazole as a potent anaplastic lymphoma kinase (ALK), c-ros oncogene 1 kinase (ROS1), and pan-tropomyosine receptor kinases (Pan-TRKs) inhibitor, *J. Med. Chem.* 59 (2016) 3392–3408.
- [21] E. Ardini, M. Menichincheri, P. Banfi, R. Bosotti, C. De Ponti, R. Pulci, D. Ballinari, M. Ciomei, G. Texido, A. Degrassi, N. Avanzi, N. Amboldi, M.B. Saccardo, D. Casero, P. Orsini, T. Bandiera, L. Mologni, D. Anderson, G. Wei, J. Harris, J.M. Vernier, G. Li, E. Felder, D. Donati, A. Isacchi, E. Pesenti, P. Magnaghi, A. Galvani, Entrectinib, a pan-TRK, ROS1, and ALK inhibitor with activity in multiple molecularly defined cancer indications, *Mol. Canc. Therapeut.* 15 (2016) 628–639.
- [22] Y. Duan, J. Wang, S. Zhu, Z.C. Tu, Z. Zhang, S. Chan, K. Ding, Design, synthesis, and Structure-Activity Relationships (SAR) of 3-vinylindazole derivatives as new selective tropomyosin receptor kinases (Trk) inhibitors, *Eur. J. Med. Chem.* 203 (2020) 112552.
- [23] A. Drilon, T.W. Laetsch, S. Kummar, S.G. DuBois, U.N. Lassen, G.D. Demetri, M. Nathanson, R.C. Doebele, A.F. Farago, A.S. Pappo, B. Turpin, A. Dowlati, M.S. Brose, L. Mascarenhas, N. Federman, J. Berlin, W.S. El-Deiry, C. Baik, J. Deeken, V. Boni, R. Nagasubramanian, M. Taylor, E.R. Rudzinski, F. MericBernstam, D.P.S. Sohal, P.C. Ma, L.E. Raez, J.F. Hechtman, R. Benayed, M. Ladanyi, B.B. Tuch, K. Ebata, S. Cruickshank, N.C. Ku, M.C. Cox, D.S. Hawkins, D.S. Hong, D.M. Hyman, Efficacy of Larotrectinib in TRK fusion-positive cancers in adults and children, *N. Engl. J. Med.* 378 (2018) 731–739.
- [24] R.C. Doebele, L.E. Davis, A. Vaishnavi, A.T. Le, A. Estrada-Bernal, S. Keyser, A. Jimeno, M. Varella-Garcia, D.L. Aisner, Y. Li, J. Stephens, D. Morosini, B.B. Tuch, M. Fernandes, N. Nanda, J.A. Low, An oncogenic NTRK fusion in a patient with soft-tissue sarcoma with response to the tropomyosin-related kinase inhibitor LOXO-101, *Canc. Discov.* 5 (2015) 1049–1057.
- [25] T.W. Laetsch, S.G. DuBois, L. Mascarenhas, B. Turpin, N. Federman, C.M. Albert, R. Nagasubramanian, J.L. Davis, E. Rudzinski, A.M. Feraco, B.B. Tuch, K.T. Ebata, M. Reynolds, S. Smith, S. Cruickshank, M.C. Cox, A.S. Pappo, D.S. Hawkins, Larotrectinib for paediatric solid tumours harbouring NTRK gene fusions: phase 1 results from a multicentre, open-label, phase 1/2 study, *Lancet Oncol.* 19 (2018) 705–714.
- [26] H.P. Su, K. Rickert, C. Burlein, K. Narayan, M. Bukhtiyarova, D.M. Hurzy, C.A. Stump, X. Zhang, J. Reid, A. KrasowskaZoladek, S. Tummala, J.M. Shipman, M. Kornienko, P.A. Lemaire, D. Krosky, A. Heller, A. Achab, C. Chamberlin, P. Saradjian, B. Sauvagnat, X. Yang, M.R. Ziebell, E. Nickbarg, J.M. Sanders, M.T. Bilodeau, S.S. Carroll, K.J. Lumb, S.M. Soisson, D.A. Henze, A.J. Cooke, Structural characterization of nonactive site, TrkAselective kinase inhibitors, *Proc. Natl. Acad. Sci. U.S.A.* 114 (2017) E297–E306.
- [27] C. Guo, I. McAlpine, J. Zhang, D.D. Knighton, S. Kephart, M.C. Johnson, H. Li, D. Bouzida, A. Yang, L. Dong, J. Marakovits, J. Tikhe, P. Richardson, L.C. Guo, R. Kania, M.P. Edwards, E. Kraynov, J. Christensen, J. Piraino, J. Lee, E. Dagostino, C. Del-Carmen, Y.L. Deng, T. Smeal, B.W. Murray, Discovery of pyrroloaminopyrazoles as novel PAK inhibitors, *J. Med. Chem.* 55 (10) (2012) 4728–4739.